NASA
Technical Memorandum 87762

AVSCOM
Technical Memorandum 86-B-4

Description of the U.S. Army Small-Scale 2-Meter Rotor Test System

Arthur E. Phelps III and John D. Berry

FEBRUARY 1987

NASA

NASA
Technical Memorandum 87762

AVSCOM
Technical Memorandum 86-B-4

Description of the U.S. Army Small-Scale 2-Meter Rotor Test System

Arthur E. Phelps III and John D. Berry
Aerostructures Directorate
USAARTA-AVSCOM
Langley Research Center
Hampton, Virginia

National Aeronautics
and Space Administration

**Scientific and Technical
Information Branch**

1987

The use of trademarks or names of manufacturers in this report is for accurate reporting and does not constitute an official endorsement, either expressed or implied, of such products or manufacturers by the National Aeronautics and Space Administration.

Contents

Symbols

Unless otherwise noted, the symbols used in this report are defined as follows:

A_1	lateral component of rotor cyclic blade pitch control, deg
a_0	rotor blade coning angle, deg
a_{1s}	longitudinal component of rotor blade flapping signal, deg
B_1	longitudinal component of rotor cyclic blade pitch control, deg
b_{1s}	lateral component of rotor blade flapping signal, deg
C_T	rotor disk area-weighted thrust coefficient
C_T/σ	blade area-weighted thrust coefficient
C_1, C_2, C_3	extension of actuators 1, 2, and 3, respectively (see fig. B1)
D	diameter of rotor (see fig. 23)
D_{1A}	distance from centerline of rotor shaft to lower pivot point of actuators 1 and 3
D_{1B}	distance from centerline of rotor shaft to lower pivot point of actuator 2
D_2	radius of swash plate at actuator attachment point
R	rotor radius
S_1	input signal multiplied by sine of current angle
S_2	input signal multiplied by cosine of current angle
x	distance from plane of actuator pivot points to center of swash plate tilt
β	input signal (from flapping potentiometer)
β_0	steady offset of input signal
β_{1c}	first harmonic cosine component of input signal
β_{1s}	first harmonic sine component of input signal
β_{2c}	second harmonic cosine component of input signal
β_{2s}	second harmonic sine component of input signal
γ	swash plate lateral tilt
δ	swash plate longitudinal tilt
θ_c	rotor collective pitch angle, deg
λ	taper ratio, ratio of root chord to tip chord
μ	rotor advance ratio, ratio of free-stream speed to rotor tip speed
σ	rotor solidity
σ_T	thrust-weighted solidity
χ	phase angle
ψ	rotor azimuth angle

Abbreviations:

IEEE	Institute of Electrical and Electronics Engineers, Inc.
MMS	mast-mounted sight
2MRTS	2-meter rotor test system
TR	taper ratio

Summary

A small-scale powered rotor model was designed for use as a research tool in the exploratory testing of rotors and helicopter models. The model consists of a 29-hp rotor drive system, a four-blade fully articulated rotor, and a fuselage. Two six-component strain-gauge balances are used to provide independent measurement of the rotor and fuselage aerodynamic loads. The model was designed to be simple to operate and maintain in wind tunnels of moderate size and complexity of the type likely to be available to a large number of industry and university researchers. Commercially available standardized hardware and equipment were used to the maximum extent possible, and specialized parts were designed so that they could be fabricated by normal methods without using highly specialized tooling.

The model was used in a hover test of three rotors having different planforms and in a forward flight investigation of a 21-percent-scale model of a U.S. Army scout helicopter equipped with a mast-mounted sight. The force data obtained from the initial tests demonstrated the capability of a comparatively simple model to provide valuable information at relatively low cost. Smoke-flow studies conducted during the wind-on tests showed the usefulness of a simple, small model in gaining an understanding of the complex flow field in which a helicopter operates.

Introduction

A number of experiments have given evidence that with proper scaling, reliable rotor data can be obtained at fairly small model scale (refs. 1 to 3), and tests conducted on models of complete helicopters have been of considerable value in evaluating general performance parameters and important stability and control characteristics of new or unusual configurations. Testing of model rotors and powered helicopters has fallen historically into two very broad categories: (1) aeroelastic testing in which specific rotor properties are evaluated on a time-variant basis, and (2) aerodynamic testing in which overall rotor or complete helicopter aerodynamic properties are evaluated on a time-averaged basis. The first of these categories requires that the model rotor have a high degree of dynamic and aeroelastic fidelity with the full-scale counterpart; thus, the design and fabrication of such model rotors is, and will continue to be, an expensive and time-consuming process. The second of these areas—overall aerodynamic testing of the time-averaged properties—offers considerably more latitude in the choice of modeling parameters. Even though close modeling of the blade mass and aeroelastic properties is, of course, always desirable, a considerable amount of valuable information can be obtained with model rotors having representative, rather than specific, properties. This occurrence is particularly true for general exploratory research in such areas as overall vehicle performance, body-wake interactions, static stability and control, and lift and drag characteristics of various airframe configurations.

Other areas of study for which a representative rotor may be suitable include vortex roll-up, wake contraction, rotor inflow conditions, configuration interference effects, and similar studies in which the gross effects of a wake from a lifting rotor are of primary significance but in which higher order aeroelastic characteristics are of secondary importance or may be ignored altogether. As a result, a model designed specifically for exploratory general research testing should be less expensive, easier to maintain, and simpler to test than a more sophisticated model embodying those features that are necessary to high-fidelity aeroelastic scaling.

This report presents details of a small-scale rotor test system, designated the "2-meter rotor test system" (2MRTS), designed to be used in generalized testing of the type just described and gives a summary of some of the results obtained from initial tests in hover and simulated forward flight. The model was designed for testing in wind tunnels of moderate size and complexity of the type likely to be available to a large number of university and industrial researchers. The intended rotor diameter of approximately 6 ft is fairly small and is conducive to design and fabrication of rotor blades by the user. Although there is, of necessity, a certain amount of unique hardware in the model, items that require routine maintenance or replacement such as gears, bearings, potentiometers, control system actuator motors, and similar items are standard, commercially available units. All specialty items, such as the transmission case, rotor shaft, hub, and control actuators, have been designed for low stresses and use stainless steel for corrosion resistance; all the major components are designed so that they can be fabricated by any skilled machinist using commonly available machine tools. The control system was designed to utilize current minicomputer technology (the sort widely available to users in the technical community) and simply fabricated interfacing circuits. The entire model system is designed to be transportable for use in a variety of locations.

General Arrangement

The general arrangement of the 2-meter rotor test system (2MRTS) is shown in figures 1 to 3 and consists basically of a rotor drive system, rotor blades, and a fuselage. The rotor drive system includes an

electric motor, a transmission, rotor controls, and a rotor hub, all mounted on a soft, damped gimbal. The drive system and the gimbal are mounted on a six-component strain-gauge balance that is used to measure rotor loads; a second balance, mounted parallel to the rotor balance, supports the fuselage shell. Lubrication oil, cooling water, and electrical power are supplied to the transmission and motor from a source outside the test area.

The rotor drive system consists of a 29-hp, three-phase, variable-frequency electric motor driving a rotor shaft through a two-stage, 90° gearbox having a 4-to-1 reduction ratio. Power for the drive motor is supplied by a separate motor-generator variable-frequency unit indigenous to the test facility. Different types of rotor hubs, including fully articulated, teetering, and hingeless, may be used, but the basic system utilizes a fully articulated four-blade hub with adjustable inplane (lead-lag) dampers. All the major components of the drive system are fabricated from stainless steel, primarily 17-4 PH, except for items such as gears, bearings, and bolts that are alloy steel.

Lubrication for the transmission is provided by a pump-driven system located outside the model. Light turbine oil is drawn from a reservoir and delivered under pressure to the transmission where it is routed to appropriate locations by means of internal oil jets. A vacuum pump co-located with the oil supply system maintains a constant vacuum in an oil-purge manifold on the bottom of the transmission. Oil drawn into the purge manifold is then returned to the reservoir where the cycle is repeated. In addition to providing lubrication for the transmission, the recirculating oil system also acts as a cooling system, and therefore an oil cooler is included in the oil circuit. Both the oil flow rate and the oil pressure are adjustable over a fairly broad range in order to allow lubrication and cooling capacity to be matched to specific test requirements.

The rotor control system uses three electromechanical actuators to position a swash plate that determines collective and cyclic control of rotor blade pitch. A minicomputer linked to the control console combines the individual actuator position signals to establish a desired collective or cyclic control position. Various levels of control logic are available to the model operator—from individual manual control of each actuator through the use of "on-off" switches to fully computer-controlled sequencing of both collective and cyclic control modes over a specified test range.

The transmission, drive motor, and rotor system are all mounted on a spring-gimbal system that is, in turn, mounted to the rotor balance. The gimbal provides a means of adjusting the stiffness and damping of the support system to reduce the likelihood of instabilities such as ground resonance. Gimbal damping is provided by adjustable, oil-filled, rotary viscous dampers and may be varied by either adjusting the damper internal valving or changing the mechanical advantage provided by the damper linkage.

The fuselage shell is mounted independently from the dynamic system and may be configured to represent any desired shape consistent with the requirement to have adequate internal clearance to avoid fouling between the fuselage, rotor, and support system load paths. The fuselage most frequently used in the course of generalized rotor performance testing is shown in figure 1. This fuselage is a generic design discussed in reference 4 and does not represent any specific production helicopter. The shell is fabricated from fiberglass-reinforced plastic and is mounted to the model in such a way as to allow easy access to the drive system for maintenance and adjustment.

Rotor instrumentation is provided on the hub and rotor blades to allow instantaneous, real-time monitoring of blade flapping and lagging motions, in-plane and out-of-plane blade bending stresses, blade torsional stresses, and pushrod loads. Data are transferred from the rotating hub to the fixed system by means of a 36-channel slip ring assembly installed in the bottom of the rotor shaft. Temperatures are monitored at various points on the transmission and swash plate by means of thermocouples mounted directly on the points of interest. A pair of thermocouples are also used to monitor the motor armature temperatures.

Detailed Description of Subsystems

Transmission and Motor Details

The motor and transmission are shown in figure 4, and a section view of the motor and transmission assembly illustrating the various components in the drive train is presented in figure 5. The drive motor is a 29-hp, three-phase, variable-frequency motor with an integral cooling-water jacket. The motor is attached to the front of the transmission by means of a flanged motor mount containing the high-speed input-shaft oil seal. The motor armature is suspended in deep-groove ball bearings capable of resisting moderate axial loading, and the input spiral bevel gear is attached directly to the motor shaft by means of a shaft key and locknut. The motor mount is secured to the motor with bolts and dowel pins. An indexing boss on the motor mount engages a close-tolerance hole in the

transmission and locates the input spiral bevel gear in a precise position relative to the intermediate-shaft driven bevel gear. Axial position of the input spiral bevel gear is adjusted by placing shims between the back of the gear indexing boss and the front face of the high-speed oil-seal inner race.

Referring to figure 5, the first-stage gear reduction takes place at the intermediate shaft which is mounted in a pair of tapered roller bearings and incorporates the driven bevel gear and rotor shaft input pinion gear. The input spiral bevel gear and driven bevel gear are commercially available stock gears and provide a 2-to-1 reduction at the intermediate shaft. The driven bevel gear vertical position and intermediate shaft bearing preload are adjustable by means of shims placed between the upper and lower bearing caps and their respective bearings. The bearing preload is adjusted by selecting the proper thickness and number of shims to produce zero detectable axial play in the intermediate shaft and then by removing an additional 0.001 in. of shims. The vertical position of the driven bevel gear is then set by adjusting the relative distribution of shims between the upper and lower bearing caps while maintaining the total shim thickness determined for the proper bearing preload.

The second-stage 2-to-1 gear reduction occurs between the rotor shaft input pinion and the rotor shaft spur gear. Both of these spur gears are fabricated from case-hardened SAE 9310 steel and incorporate a modified tooth form designed to reduce tooth stresses under the vibratory loading that may be expected in the normal course of rotor testing. The input pinion gear is machined integrally with the intermediate shaft, whereas the rotor shaft spur gear is a separate part mounted on the shaft by means of a Woodruff key, spacers, and the rotor shaft lower-bearing locknut.

The rotor shaft is supported in the transmission by means of three bearings. A pair of tapered roller bearings in the shaft bearing tower resists shaft vertical loads, and a large roller bearing in the bottom of the lower half of the transmission case provides resistance to shaft bending moments. Because the upper pair of tapered roller bearings resists both positive and negative axial loads, it is possible to test hingeless rotors under conditions of negative lift.

The transmission case is fabricated from 17-4 PH stainless steel and is made in three major parts: (1) transmission case lower half, (2) transmission case upper half, and (3) rotor shaft bearing tower. The upper and lower transmission case halves are bolted together with a close-tolerance fit using three dowel pins to position the two case halves. An indexing boss on the lower side of the bearing tower engages a hole in the upper case half and ensures proper alignment of the upper and lower rotor shaft bearings. A secondary connection between the upper and lower case halves is provided by the motor mount which uses two mounting bolts in the upper half and two bolts in the lower half.

Oil is introduced into the transmission housing through an oil supply line connected to a manifold mounted internally in the aft portion of the lower case half. A small-diameter stainless-steel tube transfers oil from the manifold and injects it directly into the mesh of the rotor shaft spur gears, and a second tube routed through the upper case half delivers oil to the rotor shaft upper bearings. As the rotor shaft spur gears mesh, excess oil is forced out axially along the gear teeth. The oil ejected at the top of the gear mesh impinges directly on the intermediate shaft upper bearing, and the oil ejected at the bottom of the spur gear mesh is directed downward onto the driven spiral bevel gear. Oil that flows down through the rotor shaft upper bearings is deposited on the top surface of the rotor shaft spur gear where centrifugal force causes it to be splashed throughout the transmission case.

As oil flows down to the bottom of the transmission, it collects in the bottom of the case and passes through the lower bearings into the intermediate shaft lower bearing cap, and into the rotor shaft lower bearing boss just above the rotor shaft lower oil seal. An oil purge port is located in the front of the lower transmission case, and a vacuum manifold is attached to the purge port. Oil is removed from the intermediate shaft bearing cap and rotor shaft lower bearing boss by means of flexible tubing connected to the vacuum manifold, and oil in the bottom of the transmission case is removed through the port at the front of the case. All oil is then returned to the reservoir through a single line. If required, the oil is passed through an oil cooler before being returned to the reservoir.

Rotor-Hub Details

The basic rotor hub used on the 2MRTS is a fully articulated, four-blade hub with adjustable in-plane damping and is shown in figures 6 to 9. The hub has coincident flap and lag hinges located at the 2-in. radial station and may be assembled with various pitch-horn offsets to provide a range of pitch-flap coupling ratios. The hub is constructed almost entirely of 17-4 PH stainless steel and is designed for the operation of model rotor blades at full-scale tip speeds and at centrifugal force levels up to 2300 lb, measured at the lead-lag hinge.

The bearings used for the flapping and lead-lag hinges are commercially available bushing-type

flanged bearings with a proprietary low-friction coating requiring no lubrication. The lead-lag pivot shaft is machined integrally with the blade-cuff retention block and is supported by bearings mounted in the upper and lower hub plates. The flapping pivot shaft passes through the blade-cuff retention block and is secured by a bolt passing through the feathering spindle as shown in figures 6 and 8. The blade cuff is shown in figure 8 and is mounted on the feathering spindle by means of two needle roller bearings and a needle thrust bearing retained by a high-strength bolt threaded into the spindle. Replaceable inner races are used for all the feathering bearings and lubrication fittings are provided in each cuff, as can be seen in the photographs in figure 7. Blades are mounted in the blade cuffs by means of three close-tolerance bolts.

Inplane damping is provided by small, commercially available rotary viscous dampers connected to each blade. A small sector gear attached to the blade-cuff retention block engages a drive gear mounted on the damper shaft and provides a 3.2-to-1 amplification for blade lag motion transmitted to the damper. The dampers and damper gear drive connections are shown in the photographs in figure 7, and the damper dynamic characteristics are presented in figure 9.

Damping values for the dampers may be varied by either adjusting the bypass valving inside the dampers or changing the damping fluid, or by a combination of the two. Inplane motion stops limit the blade motion to a 5° lead and a 15° lag, and droop stops limit the blade droop to 8°. No upper flapping stops are incorporated, but the blade cuff may move through 20° of positive flapping before encountering structural interference.

As shown in figure 6, the hub is mounted on the rotor shaft by means of a conical washer and barrel nut. A tapered socket on the bottom of the hub engages a mating tapered shoulder on the rotor shaft, and the conical washer seats into a tapered socket in the top of the hub. Shaft torque is transmitted to the hub through a close-tolerance key and through friction on the tapered socket at the base of the hub.

Blade flapping and lagging motions are monitored with small, high-precision potentiometers driven by means of sector gears attached to the flapping and lagging pivot shafts. Both measurements are made on the same blade; however, duplicate potentiometers and gears are installed at the opposite blade cuff primarily to preserve hub balance.

Rotor Blades

A typical rotor blade of the type used on the 2MRTS is shown in figure 10. Any type of blade construction may be employed so long as the operational limit of 2300 lb centrifugal force is preserved and blade dynamic characteristics are compatible with the dynamic drive system, but composite blades have generally proven to be the most satisfactory. The blades shown in figure 10 are of composite construction utilizing graphite prepreg cloth, polyurethane foam cores, fiberglass and epoxy external skins, and tungsten leading-edge balance weights.

In fabricating a blade of this type, a graphite laminate spar is first fabricated over a foam core and then cured in a mold. Afterward, the trailing-edge core is fabricated from low-density, self-skinning polyurethane foam and then bonded to the spar. The entire assembly is then wrapped with fiberglass cloth and epoxy resin, placed in the mold, and cured under controlled conditions of temperature and pressure. The use of such composite blade fabrication permits close control of both mass distribution and stiffness characteristics, and blades made in this manner exhibit repeatable dynamic characteristics.

Rotor Control System

Mechanical components. The main rotor control is shown in figures 11 to 13 and consists of rotating pushrods, a rotating swash plate with a scissors assembly and spherical bearing, a nonrotating swash plate, three electromechanical actuators, and an actuator mounting ring.

The three actuators are mounted 90° apart—one in front and one on each side—and determine swash plate vertical position and tilt. The actuators each consist of three main parts: (1) an actuator jack driven by an internal jackscrew, (2) a guide tower to contain and direct the actuator jack, and (3) an electric gearmotor to drive the jackscrew. A linear potentiometer mounted parallel to the guide tower, as shown in the photographs of figure 11, is used to provide a measure of actuator jack extension. Figure 12 shows the general arrangement of the actuator components.

The actuator mounting ring is secured to the rotor shaft bearing tower by clamp pressure and provides pivot points for the lower end of the actuators. The two side actuators are mounted in such a way that they can articulate from side to side but are restrained in fore-and-aft motion; this mounting arrangement allows the side actuators to serve as stationary scissors for the nonrotating swash plate. The front actuator is free to articulate both side to side and fore and aft in order to compensate for swash plate motion under conditions of combined longitudinal and lateral cyclic control inputs.

The rotating swash plate houses the swash plate ball and provides support points for four control pushrods and for the rotating scissors. The rotating

scissors maintain azimuthal alignment of the rotating swash plate with the rotor hub by means of a clamp-lock attachment to the rotor shaft and spherical rod-end bearing attachments to the swash plate.

Control forces and moments are transmitted from the fixed system to the rotating system through a pair of angular-contact ball bearings between the nonrotating swash plate and the rotating swash plate. For cyclic control inputs, angular deflection of the rotating swash plate relative to the rotor shaft takes place at the swash plate spherical ball bearing as shown in figure 13. When used in this way, the swash plate ball serves as a two-axis gimbal for cyclic inputs. For collective control inputs, the entire swash plate assembly translates vertically along the rotor shaft with the assembly sliding along the rotor shaft through the bore of the swash plate ball.

The pushrods are short columns threaded internally at each end to receive self-lubricated rod-end bearings. The top of the pushrod has a right-hand thread, and the bottom of the pushrod has a left-hand thread that allows a turnbuckle-style adjustment of pushrod length for adjusting the blade track. Locknuts and safety wire are used on all the rod-end bearings to ensure security of the system under the vibratory loads typical in model rotor testing, and strain gauges attached to one of the pushrods provide a measurement of pushrod loads.

Electronic components. An external means of mixing collective and cyclic pitch values is required because each actuator of the control system is driven independently. A small general-purpose computer is incorporated in the control system to allow flexibility in control of different hubs and pitch-change linkages. The computer used in the control system is used primarily to "mix" the collective and cyclic pitch values and to discern the three actuator values.

Figure 14 illustrates the complete control system and its three major components: (1) control console, (2) input/output system, and (3) computer. Each of the major components is currently housed separately and may be reconfigured with simple wiring changes.

The control console (fig. 14(b)) consists of displays and an operator panel that performs the following functions:

1. Displays actuator drive information, computed collective and cyclic values (θ_c, A_1, and B_1), and resolved flapping values (a_0, a_{1s}, and b_{1s}).
2. Accepts operator inputs for mode, collective, and cyclic values.
3. Resolves the hub flapping signal into its steady (coning a_0) and first Fourier components (longitudinal a_{1s} and lateral b_{1s}). (See appendix A.)

The control console contains all circuitry necessary to control the three swash plate actuators independently should any of the automated portions fault, and logic is contained in the control console to handle actuator fault conditions such as a stuck or "runaway" actuator. Faults cause the system to stop the drive signal, sound an enunciator, and trigger the system into the manual or standby mode until the operator clears the fault. The console has fault-identifying indicators for each actuator.

The input/output system is an intelligent device that processes requests for information from a host computer. It is configured for a maximum of 32 analog inputs, 64 bits of digital input, 4 tachometer or counterchannels, 32 bits of digital output, and 4 analog outputs. Signal processing is performed to distribute tachometer/timing pulses and amplify and/or filter analog inputs. The computer is a general-purpose 16-bit subminicomputer optimized for multitasking real-time control applications. Communications with the input/output system are performed via a 1978 instrument interface standard bus (IEEE-488). The control software, developed in FORTRAN 77, operates in multiple modes that are defined as follows:

1. Manual mode: The computer does not exercise control over the actuators but monitors the control console and actuator status.
2. Level 1 mode: This is the basic operational mode for the control system. The computer looks for operator requests for increasing or decreasing collective or cyclic values and computes the appropriate actuator extension to reach the requested values. It then drives the actuators to the required extension. (See appendix B for the computation of actuator lengths.)
3. Level 2 mode: This mode allows the computer terminal to replace the operator's console for collective and cyclic pitch inputs. The control system computes the required actuator position and then drives the actuators to values of collective and cyclic pitch that have been input from a terminal. This mode will allow a schedule of collective/cyclic pitch variations to be programmatically followed.
4. Level 3 mode: This mode will allow the control system to track nongeometric parameters of the operator's choosing. Such parameters might be lift, drag, side force or thrust, and given flapping angles. This mode requires that more data be available to the control system than required by the other modes.

The computer also generates various cuing displays for the model operator. Using a high-speed graphics generator, an X-Y type of display of cyclic

pitch and flapping components is generated. The graphics display improves operator sensitivity to the magnitudes of out-of-trim flight conditions and permits the operator to see instantly the response of the rotor to a particular control input.

The use of an easily programmed computer has simplified the development and enhancement of control software routines. Sufficient idle time is available using the current control method to allow additional codes to be implemented for test-specific requirements if needed. The software is constructed from discrete modules, a fact that further enhances modification and expansion of the codes.

Lubrication System

The transmission lubrication system is shown in figures 15 and 16 and provides pressurized oil and vacuum service to the model for lubrication and cooling of the drive system. The major components of the oil system consist of a 5-gal oil reservoir, an adjustable oil pressure pump, an air vacuum pump, an oil transfer pump, a vacuum tank, an oil heat exchanger, filters, electronic controls and sequencers, and various valves and fittings. A schematic diagram of the lubrication circuit is shown in figure 16.

Beginning at the oil pressure pump, oil is drawn from the reservoir and passed through a filter. After exiting the primary filter, the oil flows to the oil injection manifold in the back of the transmission. The manifold distributes the oil to the gear meshes and to the rotor shaft upper bearings; the other bearings in the transmission are splash lubricated by oil slung off the gear faces. An air vacuum pump maintains a constant vacuum of about 23 in. Hg on a 3-gal tank, and an oil return line is connected from the transmission to the vacuum tank. A second oil pump then transfers oil from the vacuum tank to the oil reservoir, where the circuit is repeated. A bypass valve in the oil return line allows oil to be routed through a water-jacket type of oil cooler as test conditions may require before it enters the vacuum tank.

The oil used in the lubrication system is a light turbine oil conforming to military specification MIL-L-26399 and has excellent lubrication and heat absorption characteristics while maintaining a high resistance to foaming when used to lubricate gears and bearings. This particular oil does not, however, have high adhesion characteristics to metal, and so it cannot be used as a preservative for long-term storage.

Gimbal System

The gimbal provides a soft, damped pitch and roll freedom to the dynamic system in order to reduce the likelihood of instabilities such as ground resonance. The gimbal is shown in figures 17 and 18 and consists of a mounting yoke, a roll spring, a pitch spring, pitch-spring links, a gimbal balance block, a damper yoke, and gimbal dampers.

Referring to figure 18, the rotor drive system is attached to the mounting yoke by two bolts that pass through bearings in the yoke and thread into the rear part of the upper half of the transmission case. One end of the pitch spring is attached to the rear of the transmission case, and the other end is connected to the aft end of the mounting yoke through two small links. Thus, pitching motion of the rotor drive system relative to the mounting yoke is restrained by the pitch spring, and rotor shaft tilt relative to the mounting yoke may be changed by inserting restraining links of different lengths at the back of the pitch spring.

A torsion bar roll spring is secured within the mounting yoke by means of a tapered shear pin at the front of the yoke, and the torsion bar extends through a needle bearing installed at the rear of the mounting yoke. The gimbal balance block is attached to the roll spring with a shear pin through the back of the roll spring and with a needle bearing at the front of the roll spring. Thus, rolling motion of the mounting yoke relative to the balance block is restrained by the roll spring, whereas the needle bearings eliminate pitching motion of the mounting yoke relative to the balance block. A six-component strain-gauge balance is installed in the gimbal balance block, and the entire system is then mounted on the model test support strut. The use of interchangeable pitching and rolling spring restraints allows the dynamic system, including the contribution of the support system, to be "tuned" to avoid resonance at operating speeds.

Damping is provided by means of a damper yoke and viscous dampers as shown in figure 17. The damper yoke consists of two arms attached to the rear end of the lower half of the transmission case and extending rearward and upward to a point parallel to the gimbal pitch axis and to either side of the roll axis. Two rotary viscous dampers are mounted to the sides of the gimbal balance block and are connected to the damper yoke by ball-end pushrods attached to short bell cranks on the damper shafts. In this way, damping is provided across both the pitch and roll springs and may be varied by changing the bell crank lengths, adjusting the internal valving in the damper, changing the damping fluid, or by any combination of these options.

Fuselage Shell

The basic body configuration developed for use in the majority of generalized rotor performance

testing is a hybrid design that is representative of configurations in common use throughout the world, but it is not a model of any specific helicopter. The fuselage skin is fabricated from fiberglass-reinforced plastic and is shown in figures 19 and 20.

The fuselage contours used on the generalized body were developed in reference 4 and were chosen so that they could be defined completely by a simple mathematical formulation, thereby easing the task of numerical modeling of the body for use in analysis. A complete definition of the body mathematical model, including a description of the modeling procedure, is presented in reference 4, and significant details of the procedures are presented in appendix C which is taken from reference 4.

Initial Testing Experience

Hover Testing

The first tests using the 2MRTS involved thrust and torque measurements in hover for a series of rotors having different blade planform geometries as shown in figure 21. Three rotor configurations were tested: (1) a rectangular planform having a swept tip and nonlinear twist distribution, (2) a tapered planform having $\lambda = 3$, and (3) a tapered planform having $\lambda = 5$. Both tapered blades had $-16°$ linear twist, and the taper began at 80 percent blade radius. All three rotors had the same thrust-weighted solidity and, for simplicity, all used an NACA 0012 airfoil section.

The primary purpose of the tests was to evaluate the gross effects of planform taper on the hovering performance and on the wake structures of the rotor; the effects of planform taper on forward flight characteristics were of secondary importance. Because the tests were exploratory in nature, no attempt was made to model any particular dynamic characteristics. The blades were designed to be very stiff in torsion and out-of-plane bending while having a representative weight so that the blade coning angle would be reasonable. The blades are fairly heavy when compared with mass-scaled blades—the Lock number is about 5.3—but not unreasonably so. The high torsional stiffness was chosen to minimize the impact of aeroelastic twist as a variable since twist has a powerful effect on hover performance. Since the blades were also to be used in some general forward flight research, they were designed to ensure noncoalescence of blade fundamental frequencies in the rotational operating range of 100 to 207 rad/sec (a 1/rev input range from 16 to 33 Hz).

Two different fabrication techniques were used for the blades and reflected two fundamentally different structural approaches. The first technique was to build a tubular steel spar that was designed to resist all the blade loading, and then a foam aerodynamic core was cast around the spar. An external layer of very thin (0.004 in.) fiberglass and epoxy resin was then applied to complete the blade. The second technique was the one described earlier in which a graphite D-spar, foam cores, and fiberglass skin were all assembled and cured in a mold. For general research blades, it was originally felt that a spar could be fabricated more readily and easily by silver soldering from a standard size of steel tubing and sheet stock, especially for rectangular blades with little or no twist. However, as the operation developed, this assumption was not true since the total amount of effort for the two techniques turned out to be about the same.

Actually, it became fairly evident that fabricating a steel spar with a twist of more than 4° and with reasonable blade-to-blade uniformity was an exceedingly frustrating task because of the difficulty of maintaining uniform twist while the spar reinforcement was silver soldered in place. The only blades fabricated with this procedure were the swept-tip blades shown in figure 21. Both the tapered blade sets were fabricated using the all-composite technique and are shown in figure 22.

The 2MRTS was set up for hover tests in the static test area of the Langley 4- by 7-Meter Tunnel as shown in figures 1 and 23. The model was mounted on a two-part strut, as shown in the figure, with the rotor located 91 in. ($h/D = 1.14$) from the test section floor. Tests were run by setting the rotational speed to a fixed value and then maintaining that speed through a range of collective pitch angles at zero cyclic pitch. The range of collective angles tested varied in 2° increments from near zero thrust up to the maximum value for which power was available from the drive motor. A range of rotor speeds from 716 to 1866 rpm (tip speeds from 250 to 650 ft/sec) was also run in order to evaluate the effect of rotational speed on the measured aerodynamic performance. Six components of force and moment data were recorded at each collective setting. An analysis of the data obtained during the test is available in reference 5.

Significant results were obtained from these tests at a cost of about 15 percent of that of past similar programs using more sophisticated models. Almost as significant as the reduction in cost was the reduction in time required to design, fabricate, and test the model blades when compared with earlier programs. Experience in those earlier studies had shown that approximately 16 to 24 months from start of design was required to obtain a set of blades for Mach-scaled, dynamically similar models. The three

sets of blades used in this preliminary investigation were designed, fabricated, and tested in a period of 6 months. Of course, most of the reduction in time and cost was the result of relaxing the requirements for dynamic scaling and, as a result, the preliminary tests could not be used to evaluate aeroelastic effects.

Wind-On Testing

The first wind-on test for which the 2MRTS was used was a 21-percent-scale model of a prototype of a U.S. Army scout helicopter equipped with a mast-mounted sight as shown in figure 24. On the full-scale aircraft the spherical sight is mounted above the rotor hub and contains sensors and electronics for target designating, sighting, and ranging. The location above the rotor hub was chosen to allow the aircraft to mask itself behind terrain features or vegetation in order to complicate its detection. The primary purpose of the investigation was to determine experimentally the gross effects of the sight on the overall aerodynamic characteristics, and particularly to evaluate the effect, if any, of the sight wake on the empennage characteristics. A secondary objective was to assess in a general way the effect of the rotor wake on the basic airframe aerodynamic characteristics. Since the primary objective was to evaluate major flow field characteristics rather than to define rotor performance parameters or to evaluate the rotor dynamic properties, the TR3 tapered blades from the hover study discussed previously were used for the rotor.

The model is shown in figures 24(c) and 24(d) mounted for testing in the Langley 4- by 7-Meter Tunnel. Figure 24(c) shows the model with the left fuselage side removed and illustrates the flexibility of the basic 2MRTS for a variety of test requirements. For this investigation, it was necessary to install the 2MRTS "backwards" so that the drive motor was toward the rear and to relocate the body balance. The 5° forward shaft tilt was accomplished by mounting the gimbal balance block on a hardback inclined 5° to the fuselage reference line. Since the control system mixing is accomplished analytically rather than mechanically, the correction of signs of the cyclic flapping control inputs due to the backward installation was a trivial matter. The tachometer trigger wheel was rotated 180° on the rotor shaft so that the 1/rev pulse occurred with the instrumented blade over the tail. The only other change required to the basic system concerned the hub-retaining nut. A new nut was designed to include a pair of angular contact ball bearings and a mounting flange for the mast-mounted sight support cone as shown in figure 24(b). A small slip ring assembly was installed inside the nonrotating sight support, and the wires were routed down the rotor shaft through a hollow, nonrotating standpipe that acted as an antitorque tube for the sight. Figure 25 shows the model operating in the tunnel both with and without the mast-mounted sight installed. The data from the test showed that the sight caused an increase in the overall drag, induced a nose-up pitching moment, and caused the aircraft to be somewhat more unstable with angle of attack than was the case for the basic aircraft configuration without the sight. An in-depth analysis of the data is available in reference 6.

There was also a quite unexpected, but very exciting, aspect to powered rotor testing that was encountered during the course of forward flight testing of the scout helicopter. Certain aspects of the drag and pitching-moment data for the configuration with the sight on suggested that at very low airspeeds, the separated wake from the spherical sight body was being entrained by the aft portion of the rotor disk, resulting in a 4/rev vibration and a large nose-up pitching moment. Smoke was injected into the settling chamber of the tunnel so that the flow field around the helicopter, including that around the mast-mounted sight, could be observed.

As it happened, the smoke produced by the smoke generator available at the time was not sufficiently dense to be of much value above tunnel speeds of around 40 knots, which corresponded to an advance ratio of about 0.10. The combined effects of tunnel speed and wake turbulence were strong enough to cause very rapid dissipation of the smoke to the point where neither photographs, movies, nor videotapes were able to record the flow, even though it was possible to see some flow field definition with the naked eye. At speeds below 40 knots, however, it appeared that smoke might be of use if proper illumination could be provided. Because of the small size of the model relative to the tunnel, the test could be run in the open test section configuration without fear of entraining the tunnel potential-flow core, and the open-jet feature of the tunnel permitted considerable flexibility in the choice of lighting for photography.

The first efforts at smoke-flow visualization were made using the normal tunnel lighting, which proved to be wholly inadequate. As a next step, two high-intensity strobe lights were placed on the camera side of the tunnel and were synchronized to the rotor by using the 1/rev tachometer trigger. This technique improved the smoke visibility somewhat, but it was still comparatively "wispy". As a final step, two additional strobe lights were mounted on the floor of the test cell on the far side of the tunnel jet to backlight the smoke flow. The lights were aimed slightly upward so that they would not shine into the

camera lens, and all four strobe lights were fired at a rate of 4/rev by using the tachometer trigger pulse from the rotor. The results of using this technique for illumination are shown in figures 26 and 27. As can be seen, the wake structure is clearly defined and details not easily seen otherwise are very distinct—such as the tip vortex path over the front of the wake for multiple blade passage.

Unfortunately, the flow visualization work had been conducted on a "noninterference" basis as a general diagnostic tool, and the final lighting and operational procedure was not identified until, quite literally, the final hour of the test program. Because of the pressure of a heavy tunnel schedule, it was not possible at that time to extend the flow visualization studies to investigate any wake phenomenon in detail. This information is presented here to illustrate the overall usefulness of a fairly simple model of this type and to document in a general way some of the results that can be obtained with such a model. Smoke flow studies appear to be one area in which a model of this size can be an extremely useful tool. This condition may be particularly true, for example, when considering the tip vortex and wake contraction parameters used in prescribed-wake analysis techniques. Presently, these wake parameters must be established experimentally, and an inexpensive means of obtaining data for these parameters for a variety of rotor configurations would be extremely attractive.

Concluding Remarks

As the demand for increased performance from helicopters has grown more intense, a greater need has developed to obtain experimental data on a broad range of parameters of a fundamental nature. Much of the necessary data can be obtained in a generalized research environment in which the dynamic characteristics of the rotor are not of primary significance but in which gross configuration aerodynamic characteristics are reasonably well-simulated by a representative rotor. By relaxing the requirement for high-fidelity dynamic scaling, it has been possible to design, build, and operate a powered helicopter model at a greatly reduced level of resource expenditures—financial, material, and human—and still study a broad array of aerodynamic problems unique to helicopters. In addition, a considerable amount of study can also be focused on more traditional aerodynamic concerns that are known to be influenced by the wake of a thrusting rotor, such as vehicle stability and control, airframe drag, ground effects, rotor/body interference effects through transition, and similar problem areas.

A major advantage in providing for reduced-cost testing of powered helicopter models is that the field of experimental study is then opened to many more researchers, with the obvious benefit of having more minds considering more solutions to the problems. The initial testing experience with the small-scale 2-meter rotor test system (2MRTS) has confirmed its usefulness as a general research tool both in hover and in forward flight, and the use of commercially available hardware and equipment has made it possible to obtain that tool at a cost approximately the same as for a fixed-wing, powered wind-tunnel model of similar size. Thus, the 2MRTS is representative of the type of model that can be built and operated by both university and industrial researchers with access to moderately sized wind tunnels and with relatively limited resources.

NASA Langley Research Center
Hampton, Virginia 23665-5225
November 5, 1986

Appendix A

Resolver for Periodic Signals

The aerodynamic lift and propulsive-force components of a rotor are controlled by rotor collective pitch and the orientation of the rotor disk relative to the flight path. The primary item of instrumentation used on the 2MRTS to determine rotor orientation is the flapping potentiometer. Since the flapping potentiometer measures blade flapping displacement relative to the rotor shaft, a nonoscillatory signal implies that there is zero flapping with some steady offset, and an oscillatory signal implies that there is some tilt of the tip path plane relative to the rotor shaft. The flapping signal itself does not, however, give any indication as to whether the tip path plane is tilted forward, backward, or to either side. Coupling the flapping signal with the rotor 1/rev pulse and the 72/rev incremental pulse train makes it possible to resolve the flapping signal into its longitudinal and lateral components. The flapping resolver is the instrument used to perform the required signal analysis, and this appendix presents the analytic approach that was chosen for implementation in the 2MRTS simplified resolver.

The system of terms used for rotor flapping in this appendix is shown in figure A1.

The resolver described here is used to determine the steady offset and first Fourier harmonic components of a periodic signal. The specific application is to determine coning (steady offset) and longitudinal and lateral tilt (first Fourier harmonic) of a helicopter rotor with flapping freedom.

Assume that the signal content may be represented by

$$\beta = \beta_0 + \beta_{1s} \sin \psi + \beta_{1c} \cos \psi + \beta_{2s} \sin 2\psi + \beta_{2c} \cos 2\psi + \text{H.O.T.} \quad \text{(A1)}$$

where H.O.T. denotes higher order terms and includes terms of 3ψ and above.

The required separation of steady and harmonic components is accomplished by using a low-pass and a high-pass filter on the measured flapping signal. The low-pass component represents the steady offset content and the high-pass component represents the harmonic content. The harmonic content is fed into a vector generator that has two outputs: one output is the signal multiplied by the sine of the current angle, and the other output is the signal multiplied by the cosine of the current angle. These signals may be represented by

$$\begin{aligned} S_1 &= (\beta - \beta_0) \sin \psi \\ S_1 &= \beta_{1s} \sin^2 \psi + \beta_{1c} \sin \psi \cos \psi \\ &\quad + \beta_{2s} \sin \psi \sin 2\psi \\ &\quad + \beta_{2c} \sin \psi \cos 2\psi + \text{H.O.T.} \end{aligned} \quad \text{(A2)}$$

and

$$\begin{aligned} S_2 &= (\beta - \beta_0) \cos \psi \\ S_2 &= \beta_{1s} \sin \psi \cos \psi + \beta_{1c} \cos^2 \psi \\ &\quad + \beta_{2s} \sin 2\psi \cos \psi \\ &\quad + \beta_{2c} \cos 2\psi \cos \psi + \text{H.O.T.} \end{aligned} \quad \text{(A3)}$$

Examination of equations (A2) and (A3) yields

$$\begin{aligned} S_1 &= \frac{1}{2} \beta_{1s} - \frac{1}{2} \beta_{1s} \cos 2\psi + \frac{1}{2} \beta_{1c} \sin 2\psi \\ &\quad + \beta_{2s} \left(\frac{1}{2} \cos \psi - \frac{1}{2} \cos 3\psi \right) \\ &\quad + \beta_{2c} \left(\frac{1}{2} \sin 3\psi - \frac{1}{2} \sin \psi \right) + \text{H.O.T.} \end{aligned} \quad \text{(A4)}$$

and, similarly,

$$\begin{aligned} S_2 &= \frac{1}{2} \beta_{1s} \sin 2\psi + \frac{1}{2} \beta_{1c} + \frac{1}{2} \beta_{1c} \cos 2\psi \\ &\quad + \beta_{2s} \left(\frac{1}{2} \sin 3\psi + \frac{1}{2} \sin \psi \right) \\ &\quad + \beta_{2c} \left(\frac{1}{2} \cos \psi + \frac{1}{2} \cos 3\psi \right) + \text{H.O.T.} \end{aligned} \quad \text{(A5)}$$

The signals S_1 and S_2 contain invariable terms proportional to β_{1s} and β_{1c}, respectively. By employing low-pass filters, the invariable values for β_{1s} and β_{1c} are obtained. A simplified block diagram of the current system is shown in figure A2.

Some difficulty may be experienced when obtaining a "current angle" signal for the vector generator. The input for the device requires a 12-bit digital word. A pulse-generator countercircuit using a phase-locked loop and 12-bit divider tied to the 1/rev pulse in the model is employed to provide the required input signal and 12-bit divider. Care must also be taken when filtering the flapping signal to ensure phase integrity with the 1/rev pulse used to generate the current angle.

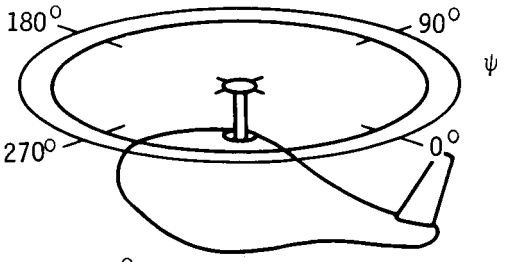

$\beta = 0^{\circ}$;
all coefficients are 0

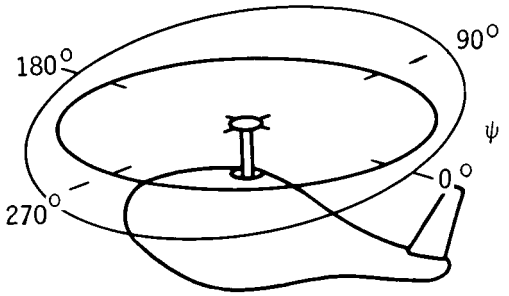

$\beta = 10 \sin \psi$, deg;
$\beta_{1s} = 10^{\circ}$;
other coefficients are 0

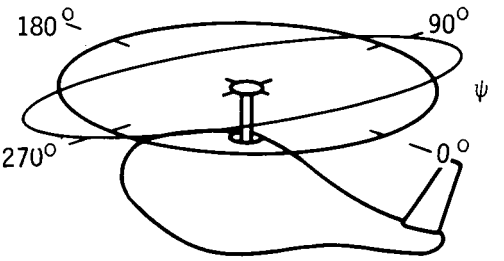

$\beta = 10 \cos \psi$, deg;
$\beta_{1c} = 10^{\circ}$;
other coefficients are 0

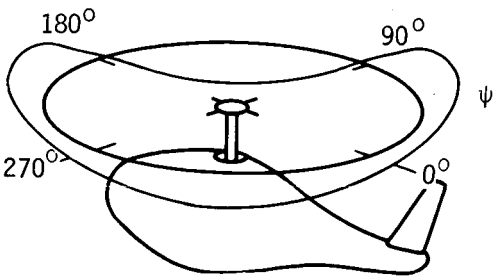

$\beta = 10 \sin 2\psi$, deg;
$\beta_{2s} = 10^{\circ}$;
other coefficients are 0

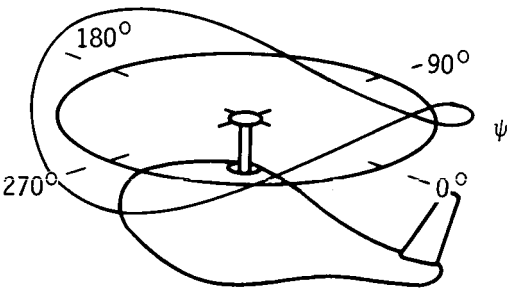

$\beta = 10 \cos 2\psi$, deg;
$\beta_{2c} = 10^{\circ}$;
other coefficients are 0

Figure A1. Flapping terms.

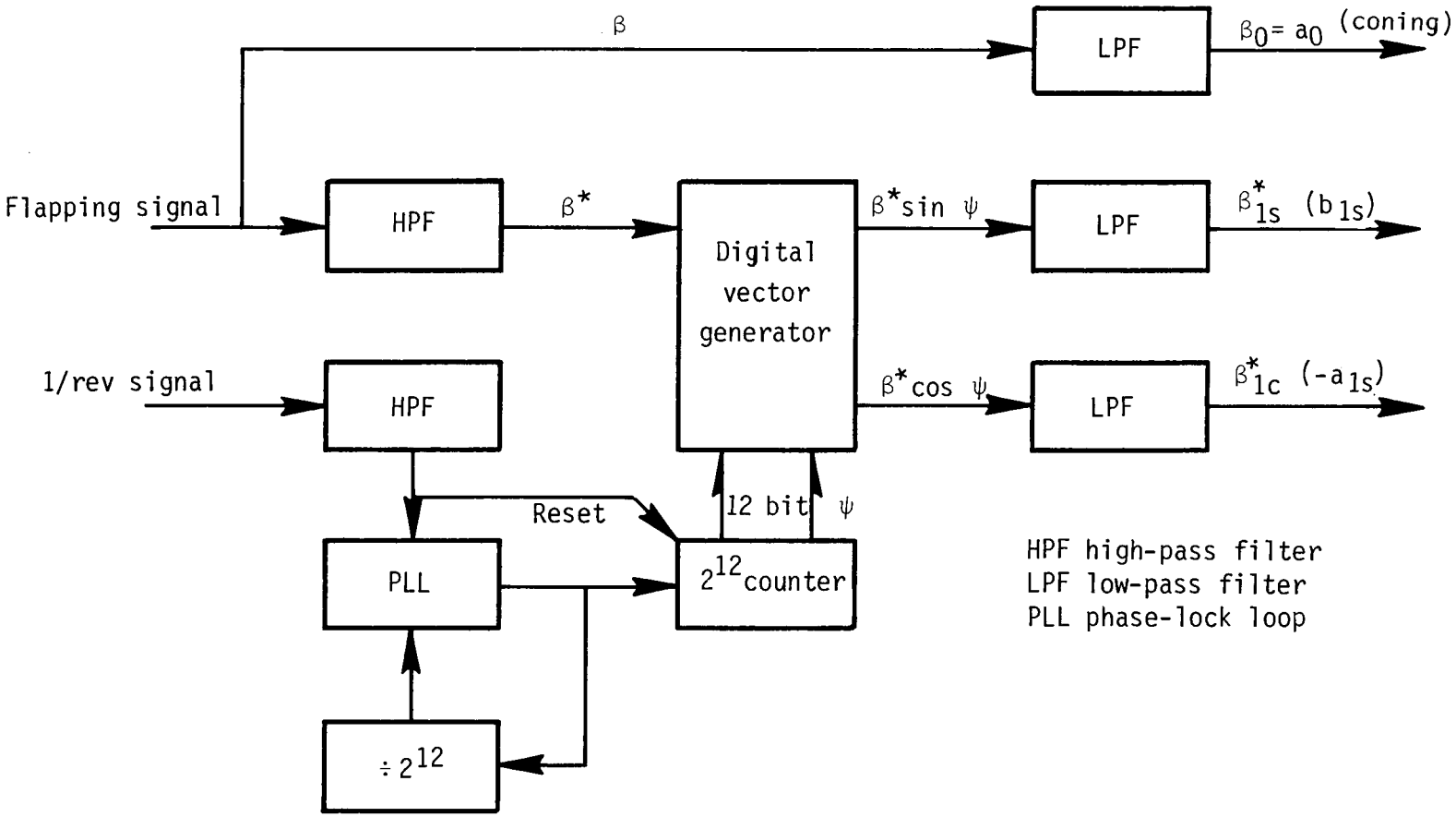

Figure A2. Block diagram of resolver system. $\beta^* = \beta - \beta_0$.

Appendix B

Control Laws

Inclination of the rotor disk plane for control and propulsion purposes is accomplished by cyclic feathering of the blade pitch, and modulation of the total rotor thrust is achieved by uniform feathering of all blades simultaneously. The physical mechanism used to accomplish the required pitch control is the swash plate, and its tilt and vertical location are established by three linear actuators. Thus, the geometries of the actuators, swash plate, and rotor hub may be used to generate a system of equations relating the actuator configuration to a specified rotor condition. Tilt of the swash plate in the axis system defined by the location of the three actuators is referred to cyclic blade pitch by an angular offset known as "phase angle". Phase angle includes the angular offset of the attachment point (the point between the pitch horn and the pushrod) from the blade feathering axis and any effective offset of the actuators from the body centerline axis. This appendix presents the derivation of the equations used by the control system logic for computing the required actuator lengths to achieve desired values of collective and cyclic pitch on the 2MRTS four-blade hub.

Swash plate tilt and vertical location determine the collective and cyclic pitch imparted to the rotor blades. Since the swash plate is centered on the rotor shaft, the collective and cyclic pitch are completely controlled by the lengths of the three actuators. The arrangement of the actuators in a 90°, 180°, and 270° pattern simplifies the mathematical relationship between actuator length and blade pitch. A computational complication is present, however, because the actuators are seldom exactly parallel to the shaft because of small initial offsets between the top and bottom actuator pivot points and because of tilting of the swash plate to generate cyclic pitch.

From the schematic arrangement shown in figure B1, the following relationships are established:

$$C_1^2 = (x - D_2 \sin\gamma)^2 + (D_2 \cos\gamma - D_{1A})^2 \quad \text{(B1)}$$

$$C_3^2 = (x + D_2 \sin\gamma)^2 + (D_2 \cos\gamma - D_{1A})^2 \quad \text{(B2)}$$

$$C_2^2 = (x - D_2 \sin\gamma)^2 + (D_2 \cos\gamma - D_{1B})^2 + (D_2 \sin\gamma \sin\delta)^2 \quad \text{(B3)}$$

Expanding gives

$$C_1^2 = x^2 + (D_2 - D_{1A})^2 + 2D_2 [D_{1A}(1 - \cos\gamma) - x \sin\gamma] \quad \text{(B4)}$$

$$C_3^2 = x^2 + (D_2 - D_{1A})^2 + 2D_2 [D_{1A}(1 - \cos\gamma) + x \sin\gamma] \quad \text{(B5)}$$

$$C_2^2 = x^2 + (D_2 - D_{1B})^2 + 2D_2 [D_{1B}(1 - \cos\delta \cos\gamma) - x \sin\delta \cos\gamma] \quad \text{(B6)}$$

These equations can be used to generate solutions for actuator extension in terms of collective and cyclic pitch values. A second relationship can be derived to solve for collective and cyclic pitch in terms of actuator extension. Thus,

$$x \sin\gamma = \frac{C_3^2 - C_1^2}{4D_2} \quad \text{(B7)}$$

$$x^2 = \frac{C_3^2 - C_1^2}{2} - (D_2 - D_{1A})^2 - 2D_2 D_{1A}(1 - \cos\gamma) \quad \text{(B8)}$$

$$\sin\delta = \frac{[x^2 (D_2 - D_{1B})^2 + 2D_2 D_{1B}(1 - \cos\delta \cos\gamma)]}{x \cos\gamma} \quad \text{(B9)}$$

These equations are solved using an iterative method.

Additional nonlinear trigonometric terms are introduced by the pushrod inclination that occurs in connecting the swash plate and blade cuff pitch horn, and these terms will probably be different for each hub-and-shaft combination. Although highly twisted blades and high collective pitch angles can cause these terms to become significant, they are not addressed here because their effect is small for the 2MRTS four-blade hub.

The particular computer system used for the control system does not execute trigometric functions efficiently; therefore, a simplified form of the equations was desired. For small γ and δ angles, a simplified linear assumption produces small errors. The simplified relations are

$$C_1^2 = x^2 + (D_2 + D_{1A})^2 - 2xD_2 \sin\gamma \quad \text{(B10)}$$

$$C_3^2 = x^2 + (D_2 + D_{1A})^2 + 2xD_2 \sin\gamma \quad \text{(B11)}$$

$$C_2^2 = x^2 + (D_2 - D_{1B})^2 + 2xD_2 \sin\delta \quad \text{(B12)}$$

With angles smaller than 10°, the simplified relations are less than ½° in error from the more rigorous trigonometric calculations.

The angles computed for swash plate tilt are in the axis system defined by the locations of the three

actuators. To relate these to cyclic feathering of blade pitch, the effective offset angle (phase angle) χ is used. Phase angle refers to the angular difference between the azimuth of applied cyclic control and the actual blade azimuth at which the blade pitch changes. Although phase angle is derived from the mechanical arrangement of the actuators and blade pitch-horn attachment points, it is more practically determined by experiment. The relation between swash plate tilt and cyclic pitch is

$$A_1 = \delta \cos \chi - \gamma \sin \chi$$

$$B_1 = \gamma \cos \chi + \delta \sin \chi$$

These derivations assume a trailing pitch-horn convention; leading pitch horns will reverse the signs used here for A_1 and B_1.

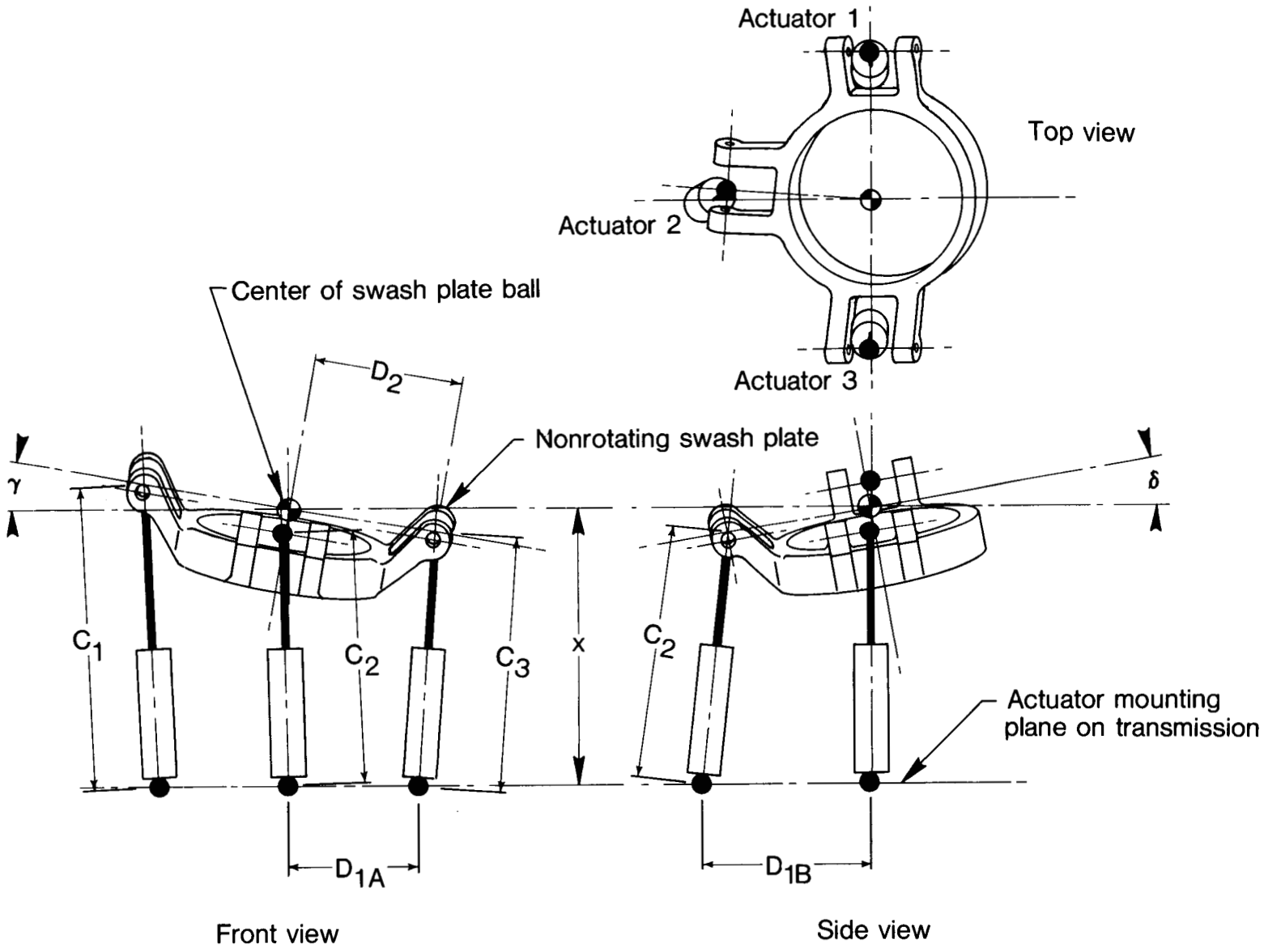

Figure B1. Control system notation and geometry used in formulation of control laws.

Appendix C

Analytic Representation of Fuselage Shapes

Based on data presented in reference 4, the fuselage shape is derived from super-ellipse equations where, for a given fuselage station (X), the cross section (Y and Z coordinates) is defined by the height (H), width (W), camber line ($Z0$), and elliptical power (N).

A super ellipse is defined by the elliptical equation

$$\left(\frac{x+x0}{A}\right)^n + \left(\frac{y+y0}{B}\right)^m = C \qquad \text{(C1)}$$

where n and m are not necessarily equal to 2 or to each other, and A, B, C, $x0$ and $y0$ are arbitrary constants. By solving for y as a function of x (i.e., $y = F(x)$), equation (C1) becomes

$$y = F(x) = B\left[C - \left(\frac{x+x0}{A}\right)^n\right]^{1/m} - y0 \qquad \text{(C2)}$$

Making the substitutions $m = C_8$, $y0 = -C_6$, $B = C_7$, $C = C_1$, and $X = x$ and by expanding the term

$$-\left(\frac{x-x0}{A}\right)^n$$

to

$$+ C_2\left(\frac{X+C_3}{C_4}\right)^{C_5}$$

equation (C2) becomes

$$F(X) = C_6 + C_7\left[C_1 + C_2\left(\frac{X+C_3}{C_4}\right)^{C_5}\right]^{1/C_8} \qquad \text{(C3)}$$

Equation (C3) is then used to calculate H, W, $Z0$, and N as a function of X by selection of an appropriate set of constants C_1 through C_8 (table CI).

The cross section at the fuselage station X can then be defined by a polar coordinate (r, ϕ) form of equation (C1) with

$$y + y0 = (r\cos\phi)^N \qquad \text{(C4)}$$

$$x + x0 = (r\sin\phi)^N \qquad \text{(C5)}$$

and the constant relations $C = 1$ and $n = m = N$. Thus, solving for r, equation (C2) becomes

$$r = \left[\frac{(AB)^N}{(A\sin\phi)^N + (B\cos\phi)^N}\right]^{1/N} \qquad \text{(C6)}$$

Therefore, the body Cartesian coordinates may be obtained for $\phi = 0$ to 2π by using equation (C6) and substituting $A = H/2, B = W/2$ and N obtained from $-\left(\frac{x+x0}{A}\right)^n$ to determine r. The Cartesian coordinates Y and Z are then calculated using $Y = r\sin\phi$ and $Z = r\cos\phi + Z0$ where $Z0$ was obtained using $-\left(\frac{x+x0}{A}\right)^n$. As shown in figure 20, the body is divided into four regions and the pylon into two regions with a set of constants for each region.

Table CI. Numerical Constants for Fuselage

[Data taken from table II of ref. 4 with some corrected data]

Function	X/R	C_1	C_2	C_3	C_4	C_5	C_6	C_7	C_8
Fuselage parameters									
H	0 to 0.4	1.0	−1.0	−0.4	0.4	1.8	0	0.25	1.8
W	↓	1.0	−1.0	−.4	↓	2.0	0	.25	2.0
$Z0$	↓	1.0	−1.0	−.4	↓	1.8	−.08	.08	1.8
N	↓	2.0	3.0	0	↓	1.0	0	1.0	1.0
H	0.4 to 0.8	0.25	0	0	0	0	0	1.0	1.0
W	↓	.25	↓	↓	↓	↓	↓	↓	↓
$Z0$	↓	0	↓	↓	↓	↓	↓	↓	↓
N	↓	5.0	↓	↓	↓	↓	↓	↓	↓
H	0.8 to 1.9	1.0	−1.0	−0.8	1.1	1.5	0.05	0.2	0.6
W	↓	1.0	−1.0	↓	↓	1.5	.05	.2	.6
$Z0$	↓	1.0	−1.0	↓	↓	1.5	.04	−.04	.6
N	↓	5.0	−3.0	↓	↓	1.0	0	1.0	1.0
H	1.90 to 2.00	1.0	−1.0	−1.9	0.1	2.0	0	0.05	2.0
W	↓	1.0	−1.0	−1.9	.1	2.0	↓	.05	2.0
$Z0$	↓	.04	0	0	0	0	↓	1.0	1.0
N	↓	2.0	0	0	0	0	↓	1.0	1.0
Pylon parameters									
H	0.4 to 0.8	1.0	−1.0	0.8	0.4	3.0	0	0.2	3.0
W	↓	1.0	−1.0	−.8	.4	3.0	↓	.172	3.0
$Z0$	↓	.122	0	0	0	0	↓	1.0	1.0
N	↓	5.0	0	0	0	0	↓	1.0	1.0
H	0.80 to 1.018	1.0	−1.0	−0.8	0.218	2.0	0	0.2	2.0
W	↓	1.0	−1.0	−.8	.218	2.0	0	0.172	2.0
$Z0$	↓	1.0	−1.0	−.8	1.1	1.5	.065	0.06	.6
N	↓	.122	0	0	0	0	0	1.0	1.0

References

1. Fradenburgh, Evan A.: Aerodynamic Design of the Sikorsky S-76 Helicopter. Preprint No. 78-06, *34th Annual National Forum*, American Helicopter Soc., Inc., May 1978.
2. Balch, David T.: Full-Scale Wind Tunnel Tests of a Modern Helicopter Main Rotor—Correlation With Model Rotor Test Data and With Theory. Preprint No. 78-03B, *Proceedings of the 34th Annual National Forum*, American Helicopter Soc., May 1978.
3. Keys, Charles N.; McVeigh, Michael A.; Dadone, Leo; and McHugh, Francis J.: Considerations in the Estimation of Full-Scale Rotor Performance From Model Rotor Test Data. *Proceedings of the 39th Annual Forum of the American Helicopter Society*, May 1983, pp. 34–43.
4. Freeman, Carl E.; and Mineck, Raymond E.: *Fuselage Surface Pressure Measurements of a Helicopter Wind-Tunnel Model With a 3.15-Meter Diameter Single Rotor.* NASA TM-80051, 1979.
5. Phelps, Arthur E., III; and Althoff, Susan L.: *Effects of Planform Geometry on Hover Performance of a 2-Meter-Diameter Model of a Four-Bladed Rotor.* NASA TM-87607, AVSCOM TR 85-B-6, 1986.
6. Phelps, Arthur E., III; and Berry, John D.: *Wind-Tunnel Evaluation of a 21-Percent-Scale Powered Model of a Prototype Advanced Scout Helicopter.* NASA TP-2420, AVSCOM TR 85-B-2, 1985.

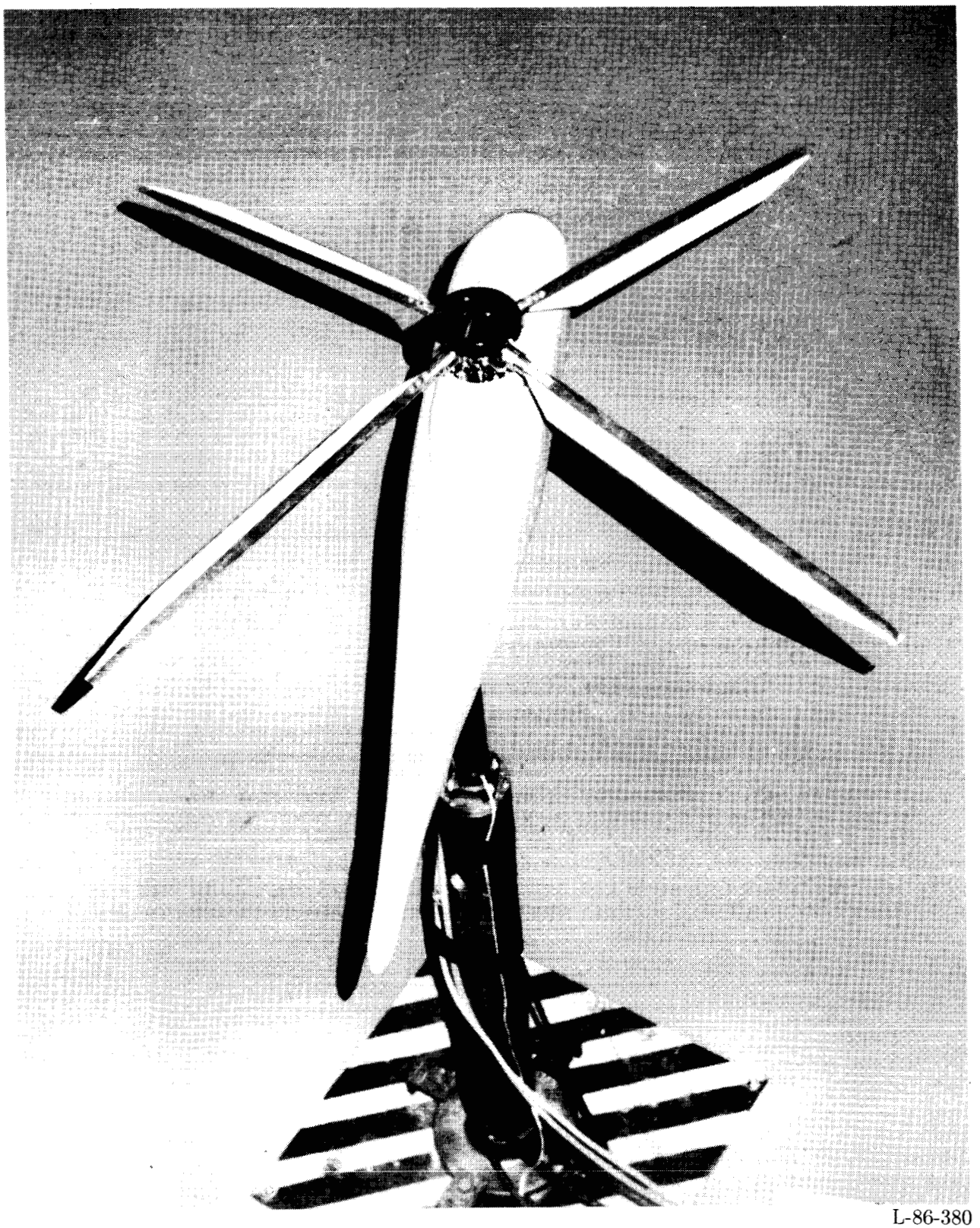

L-86-380

Figure 1. Top rear view of the 2-meter rotor test system (2MRTS) mounted for hover testing.

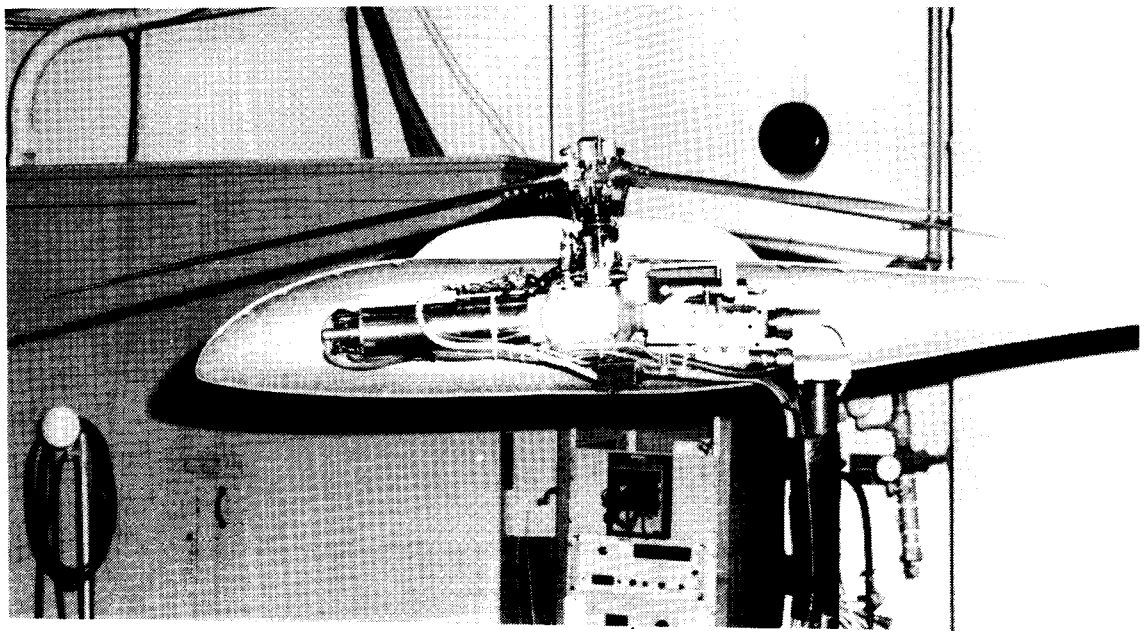

L-83-731

(a) General research configuration.

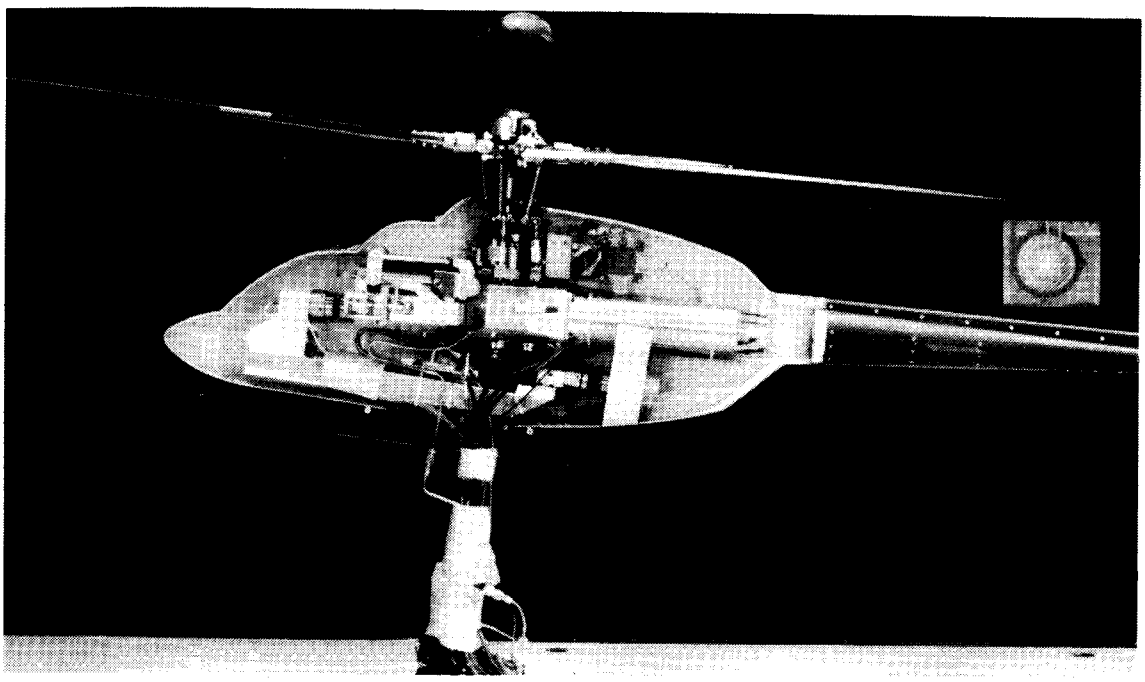

L-84-306

(b) U.S. Army scout helicopter configuration.

Figure 2. The 2MRTS with left fuselage half removed to show arrangement of drive system, gimbal, and strain-gauge balances.

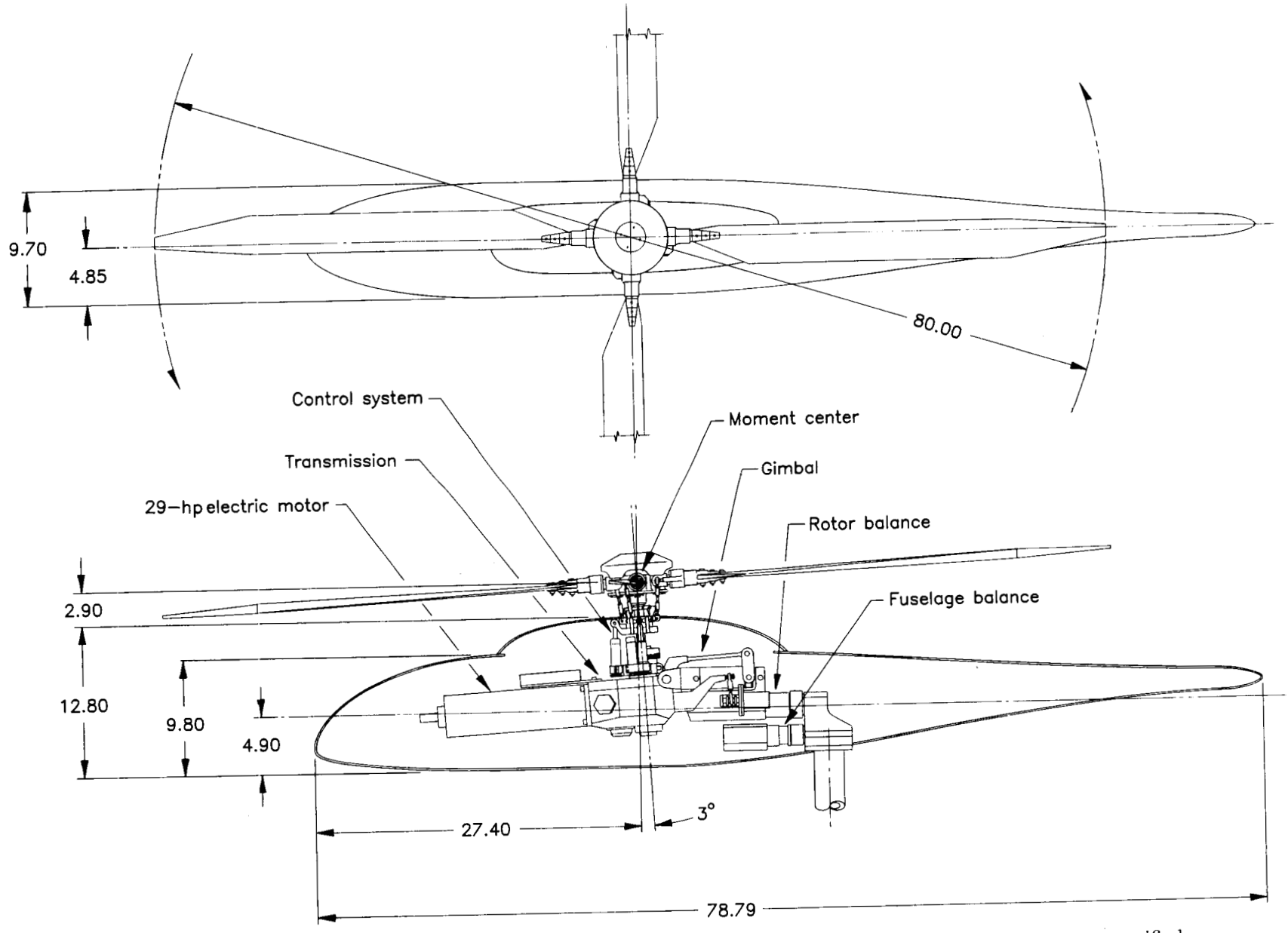

Figure 3. General arrangement of 2MRTS components. Dimensions are given in inches unless otherwise specified.

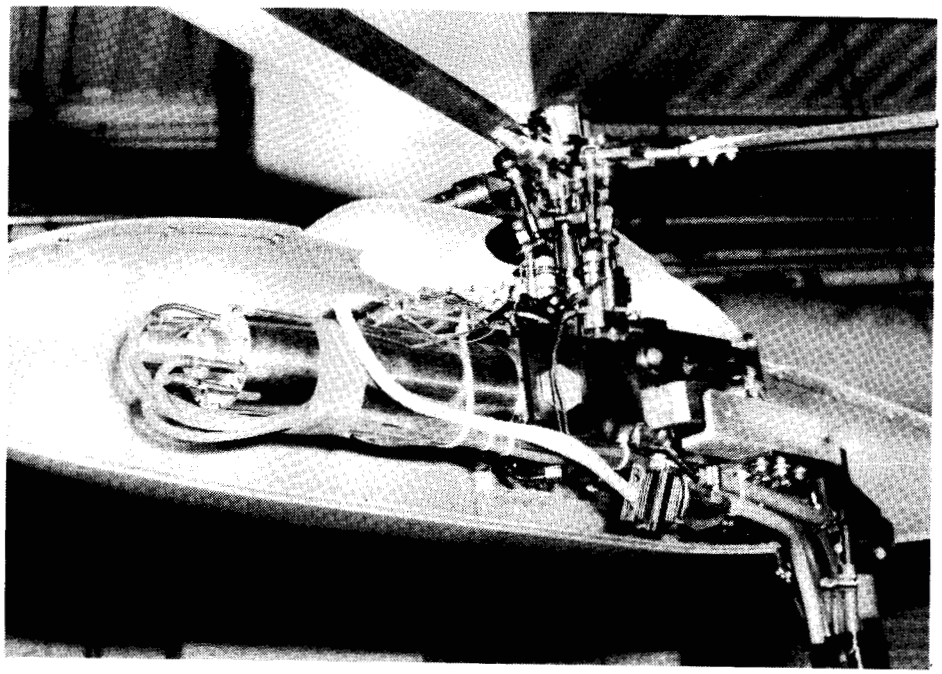

L-83-730

(a) Three-quarter front view.

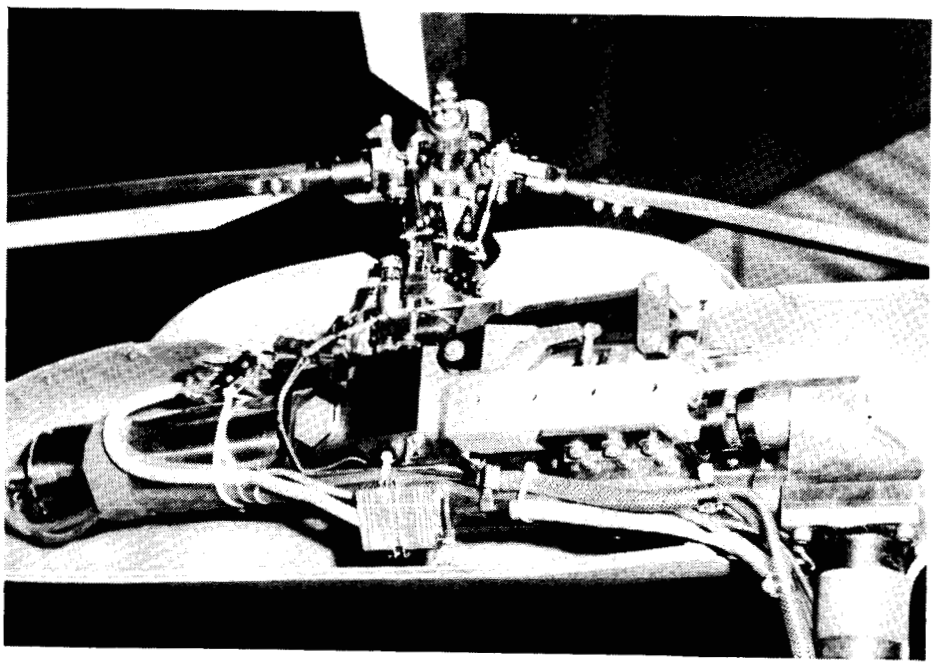

L-83-724

(b) Three-quarter rear view.

Figure 4. General arrangement of the 2MRTS.

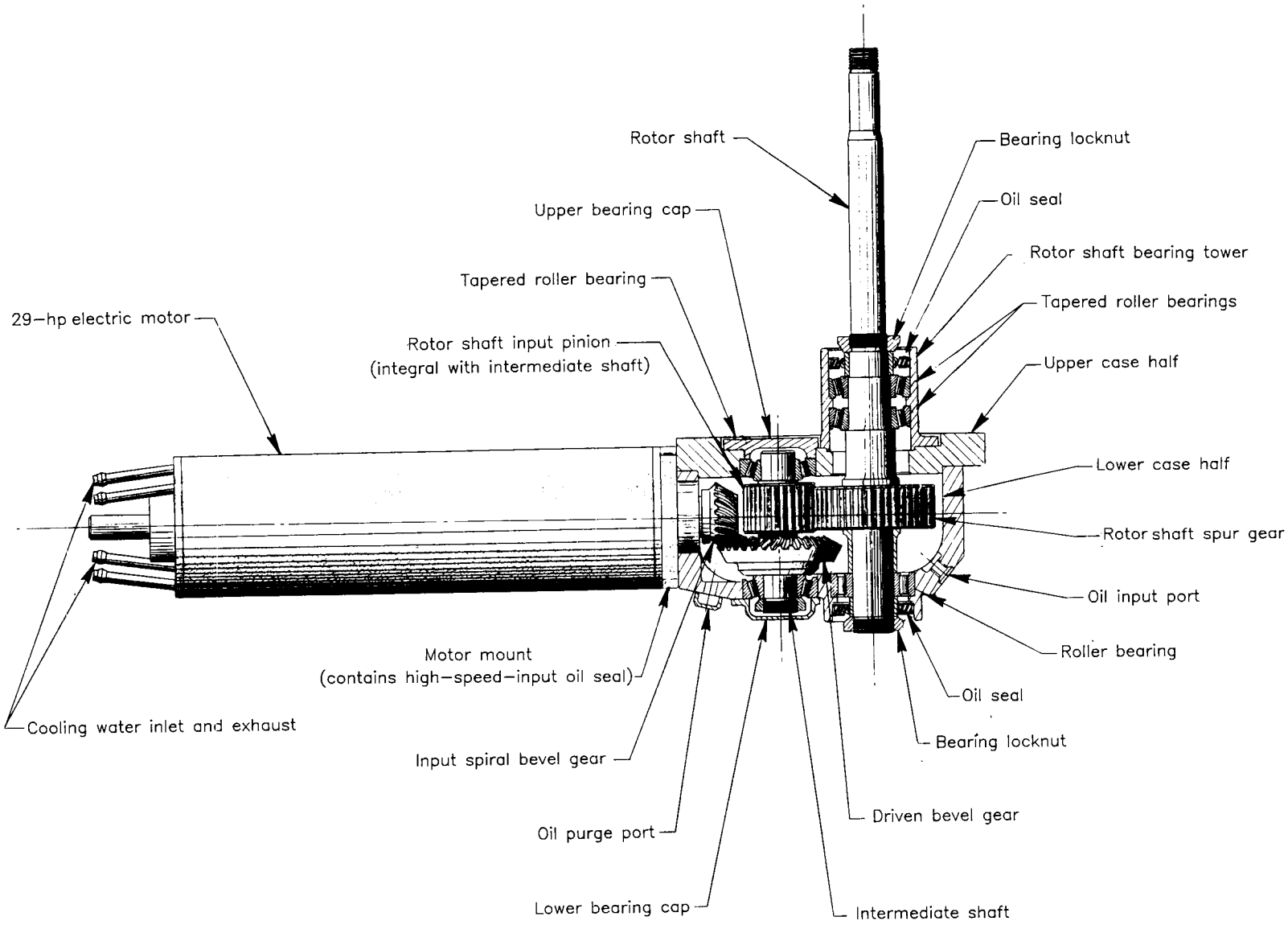

(a) General arrangement.

Figure 5. Transmission details.

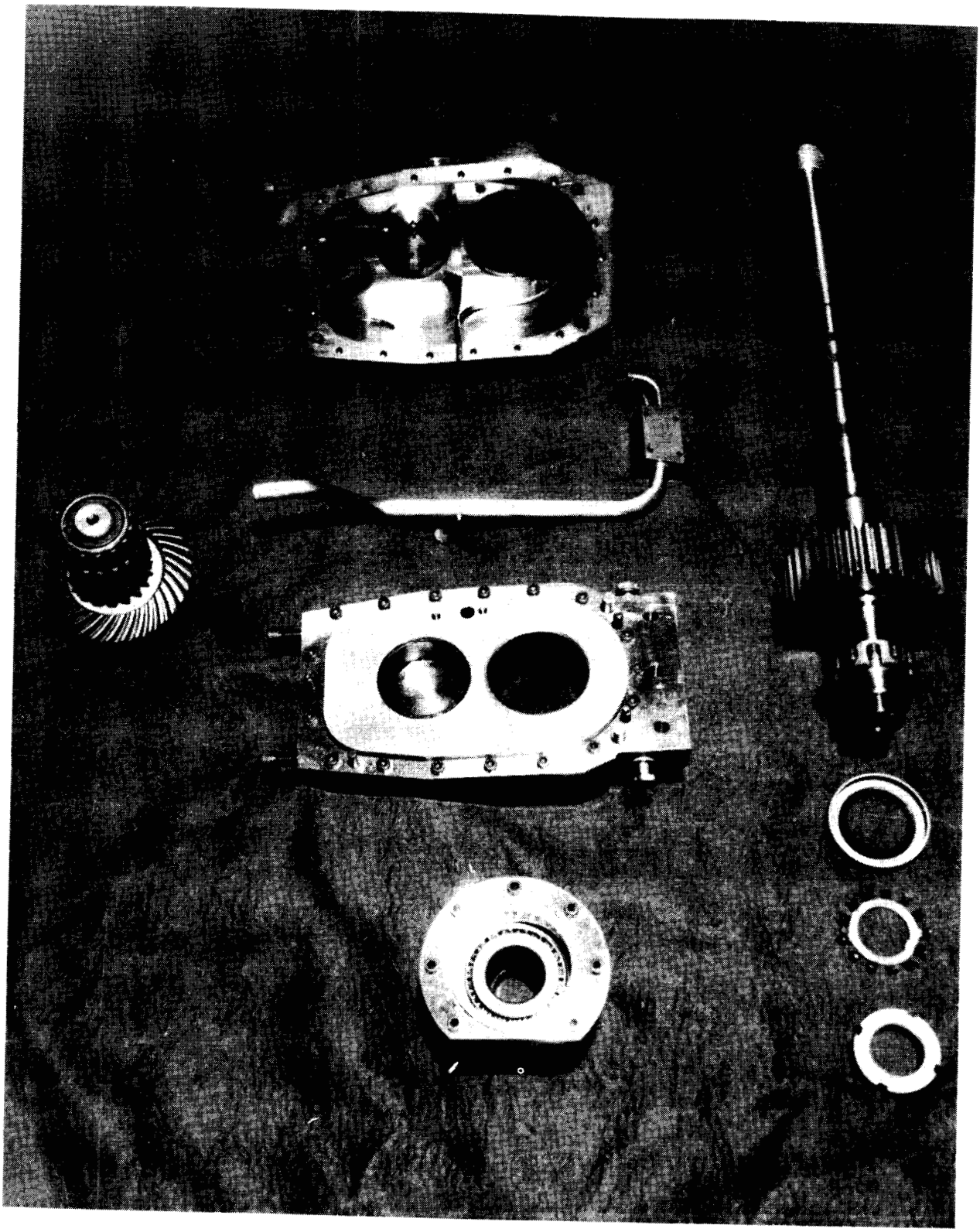

L-86-381

(b) Transmission components.

Figure 5. Continued.

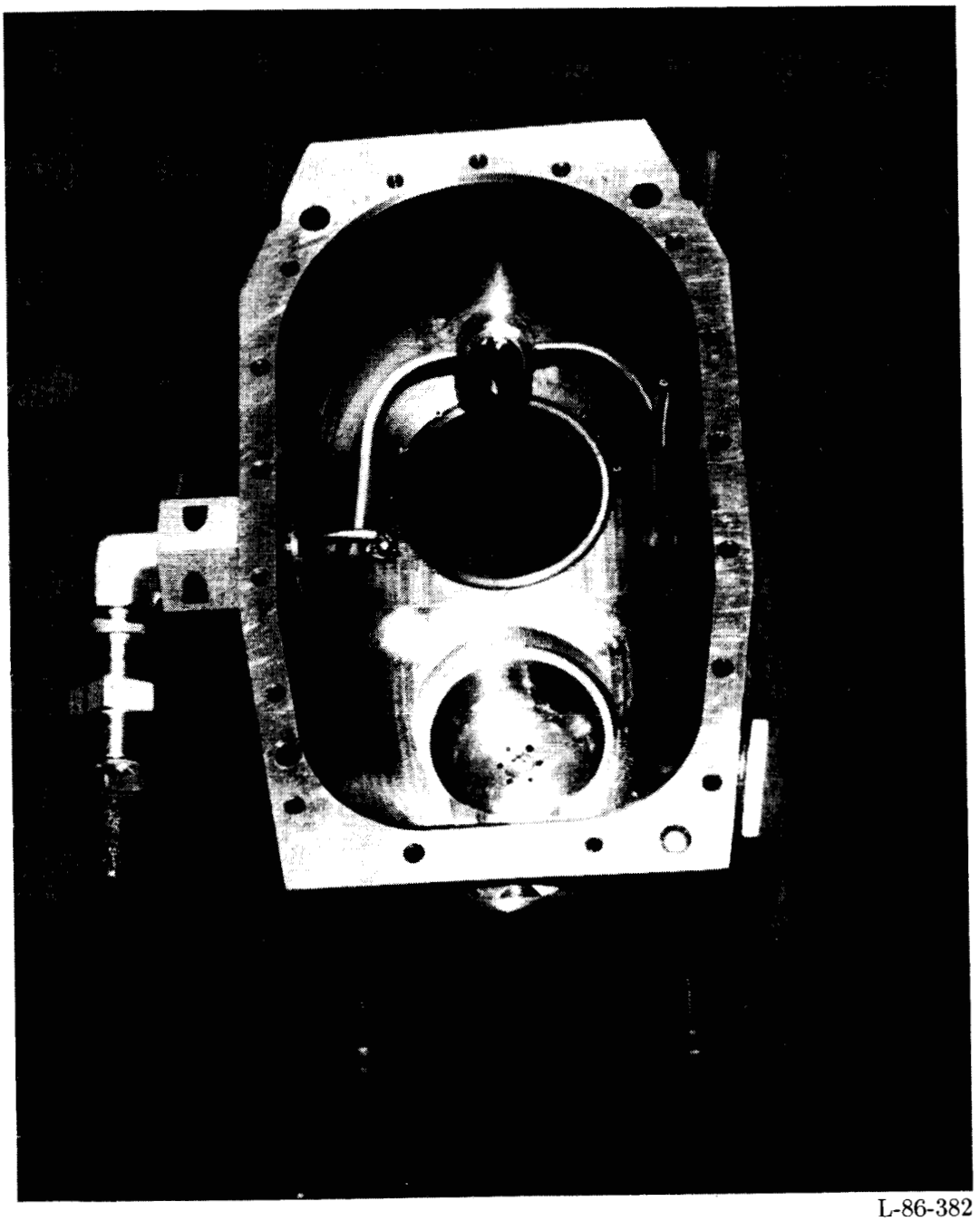

L-86-382

(c) Installation of oil manifold.

Figure 5. Continued.

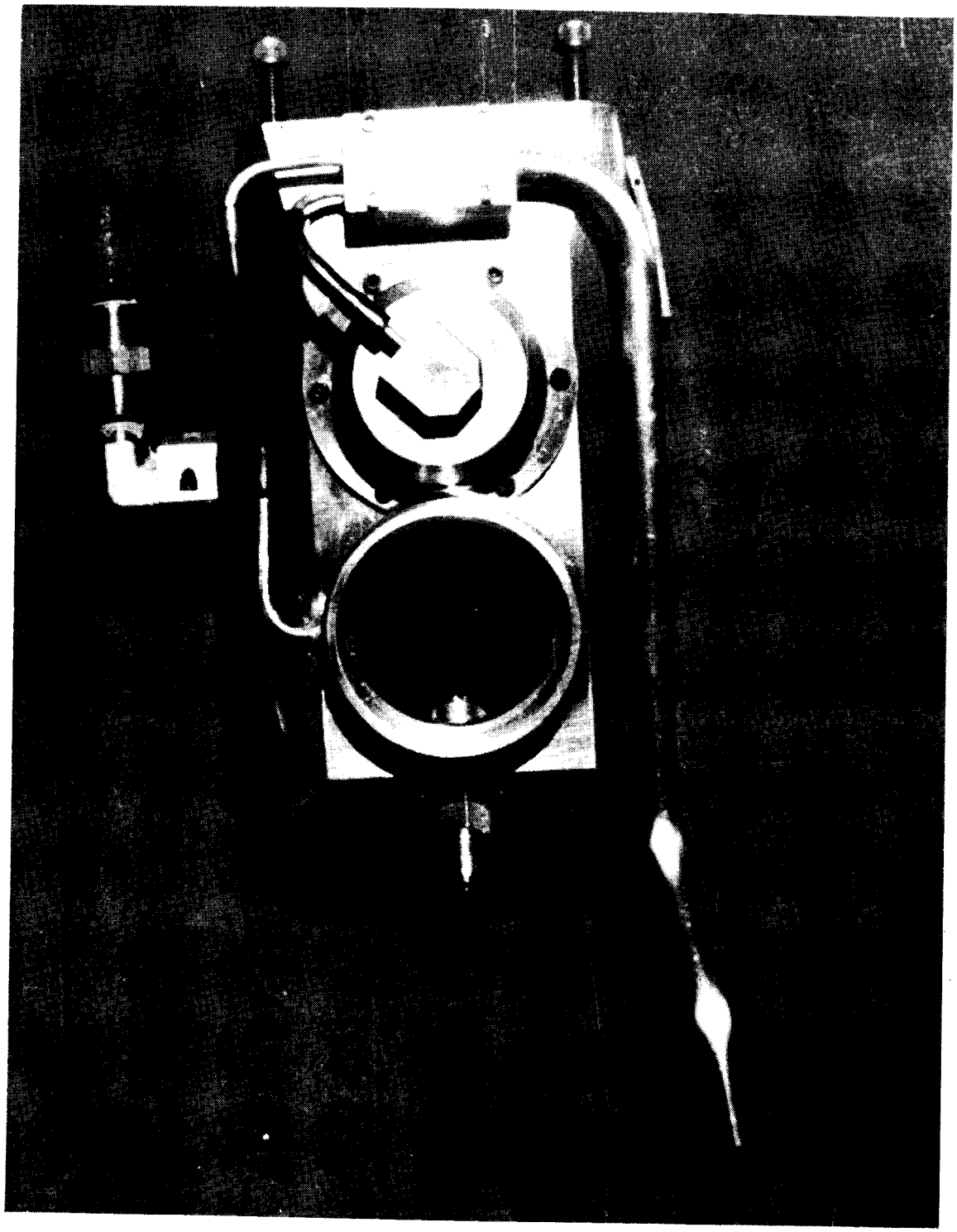

L-86-383

(d) Oil-removal vacuum manifold.

Figure 5. Continued.

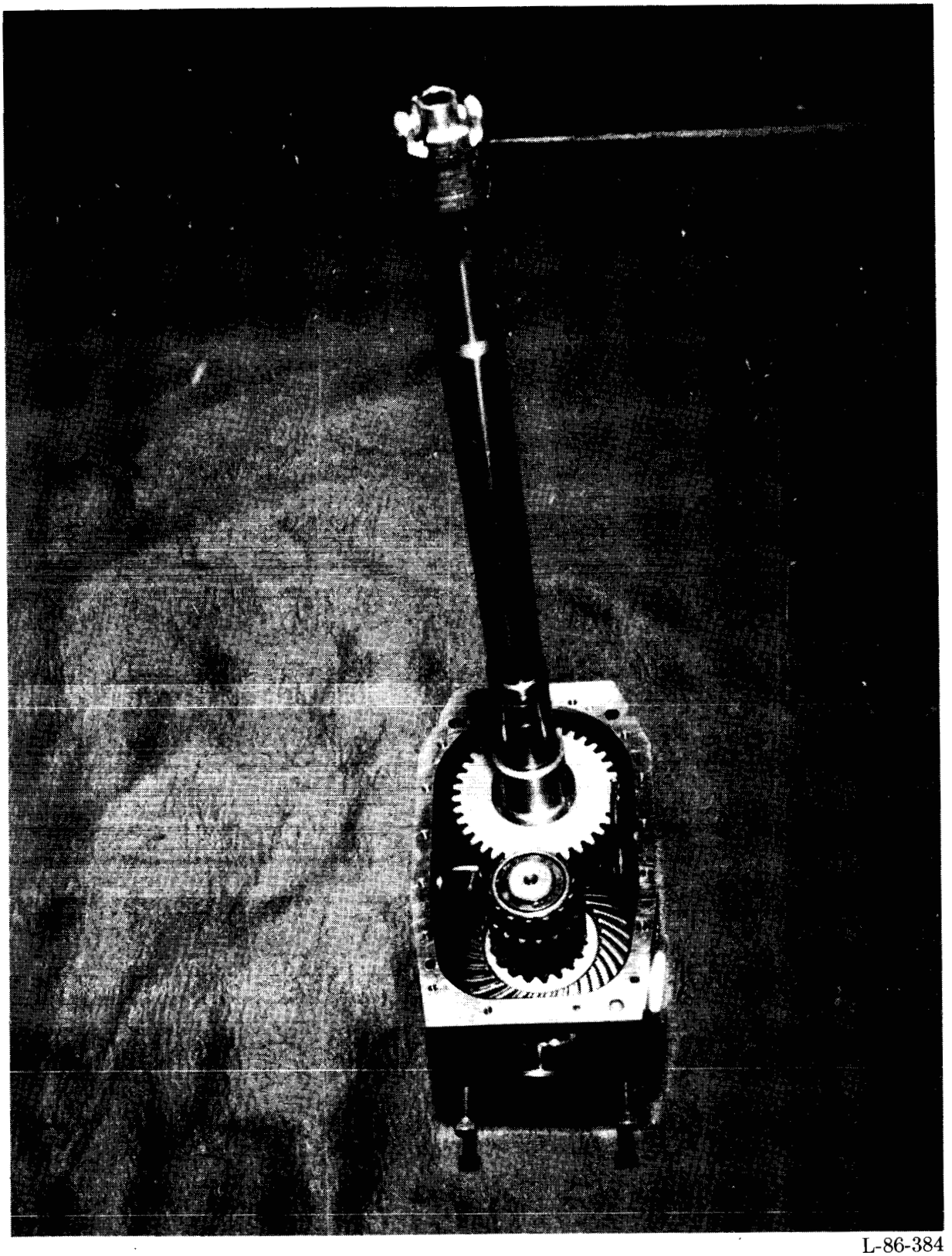

L-86-384

(e) Transmission gear train.

Figure 5. Continued.

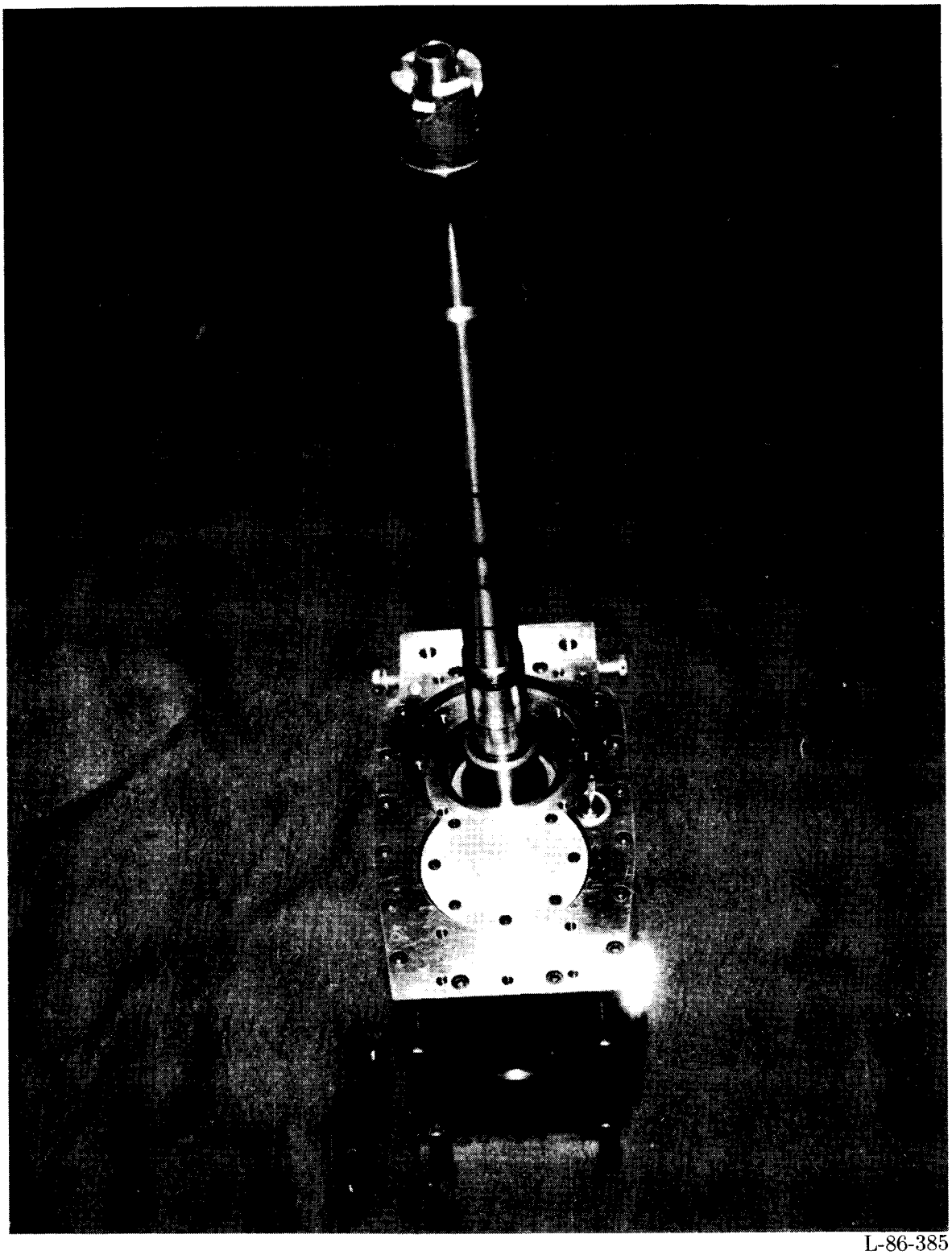

L-86-385

(f) Assembled transmission.

Figure 5. Continued.

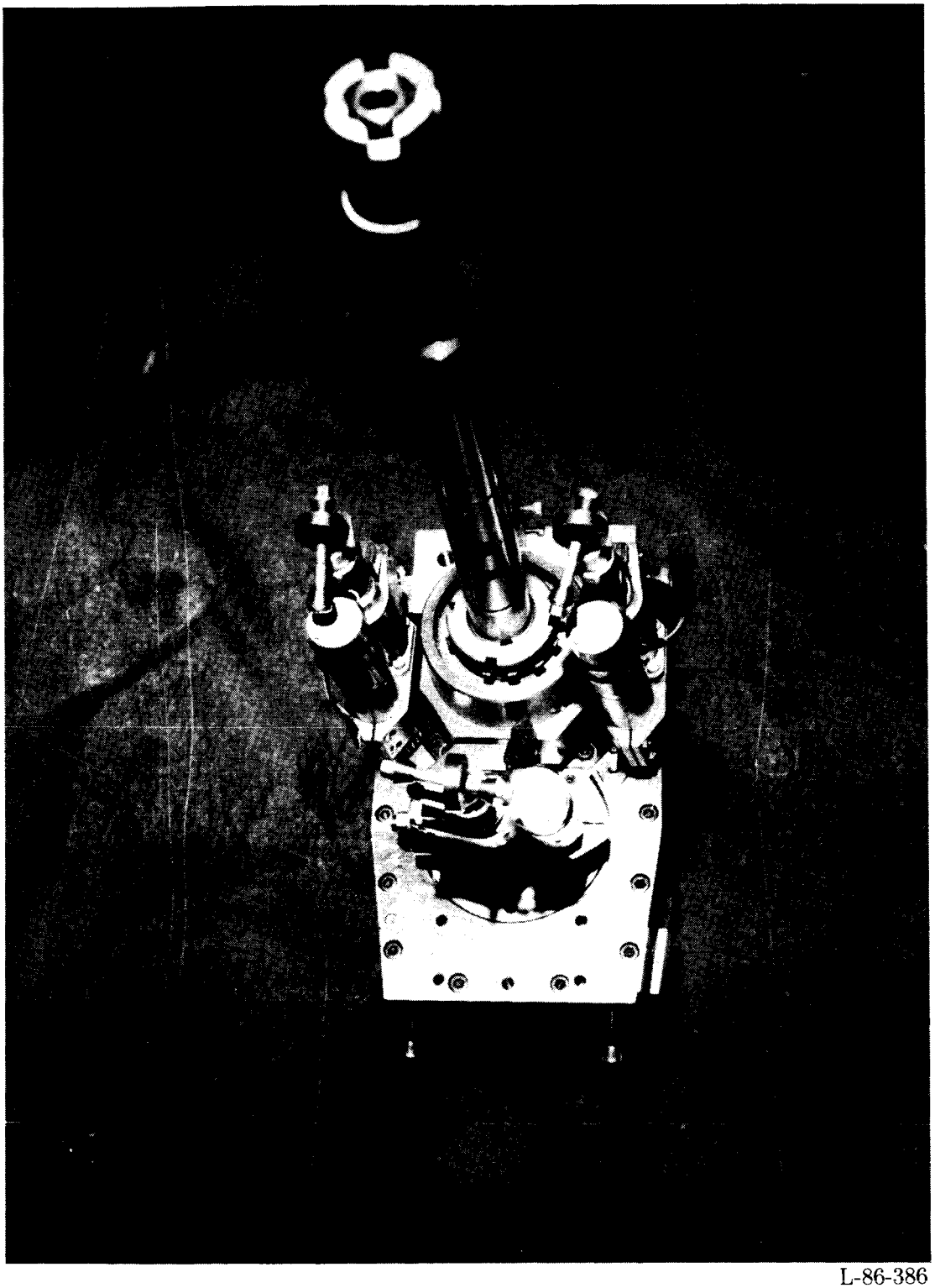

L-86-386

(g) Control system installed on rotor shaft bearing tower.

Figure 5. Concluded.

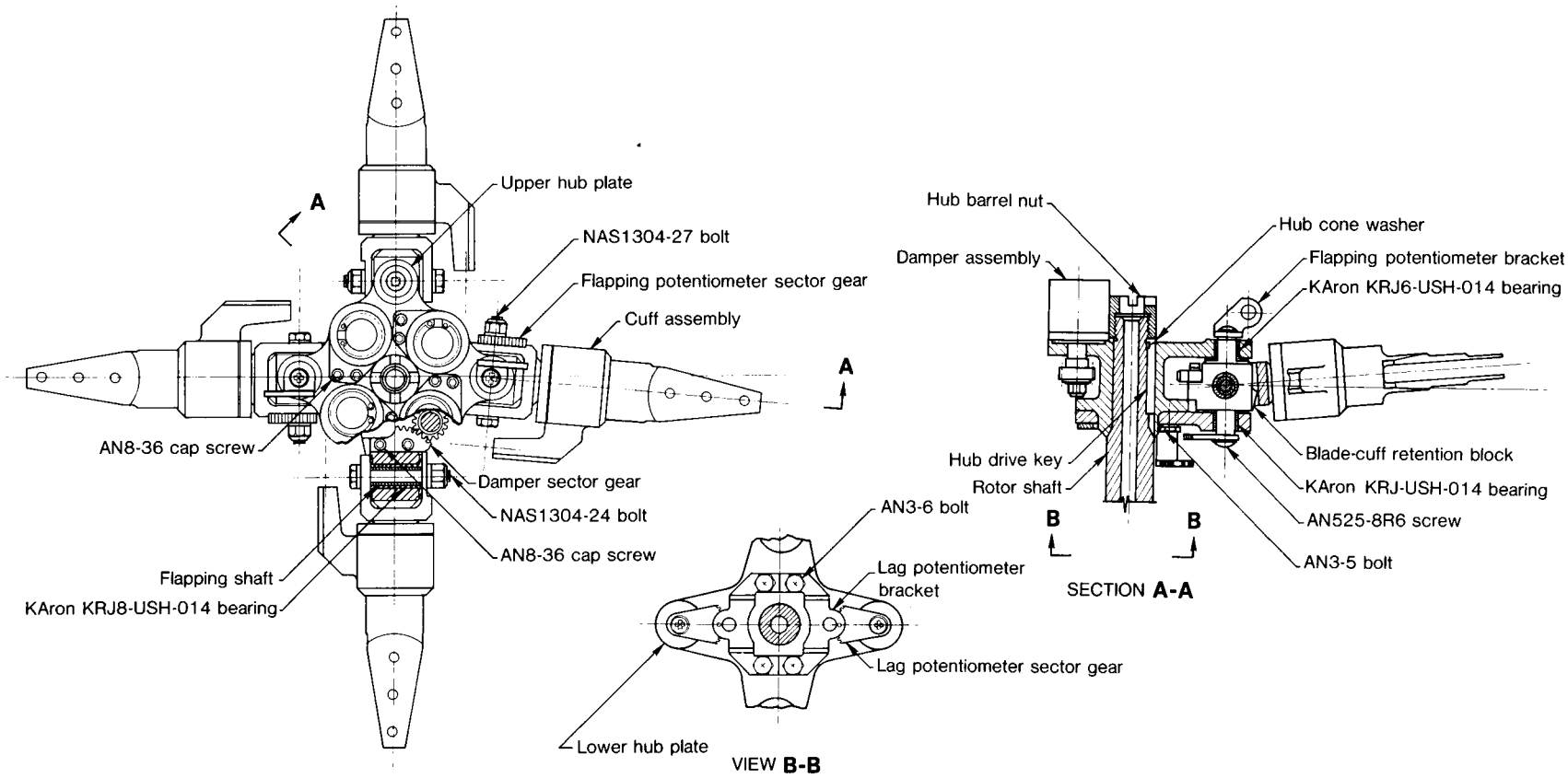

Figure 6. General arrangement of four-blade articulated hub. (KAron is a registered trademark of the Kamatics Corporation.)

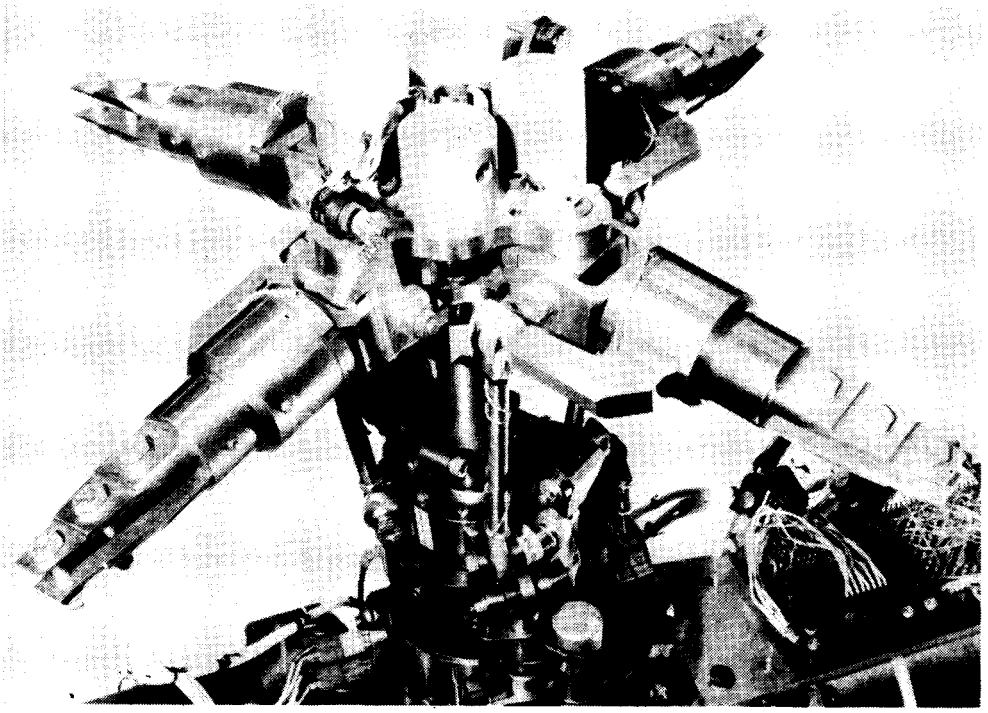

L-84-5546

(a) Three-quarter top view.

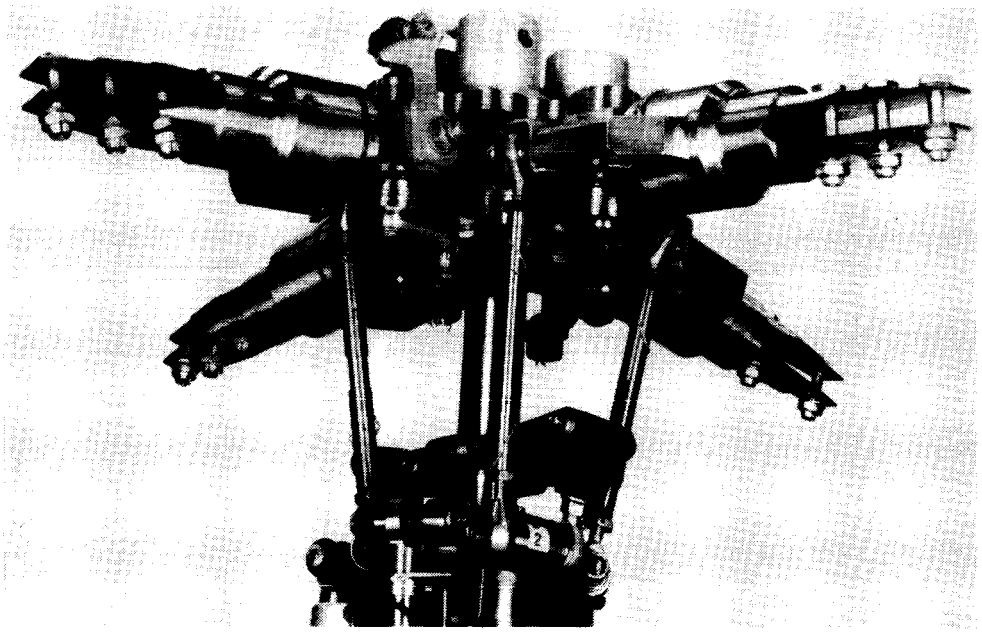

L-84-5547

(b) Three-quarter bottom view.

Figure 7. Four-blade articulated hub.

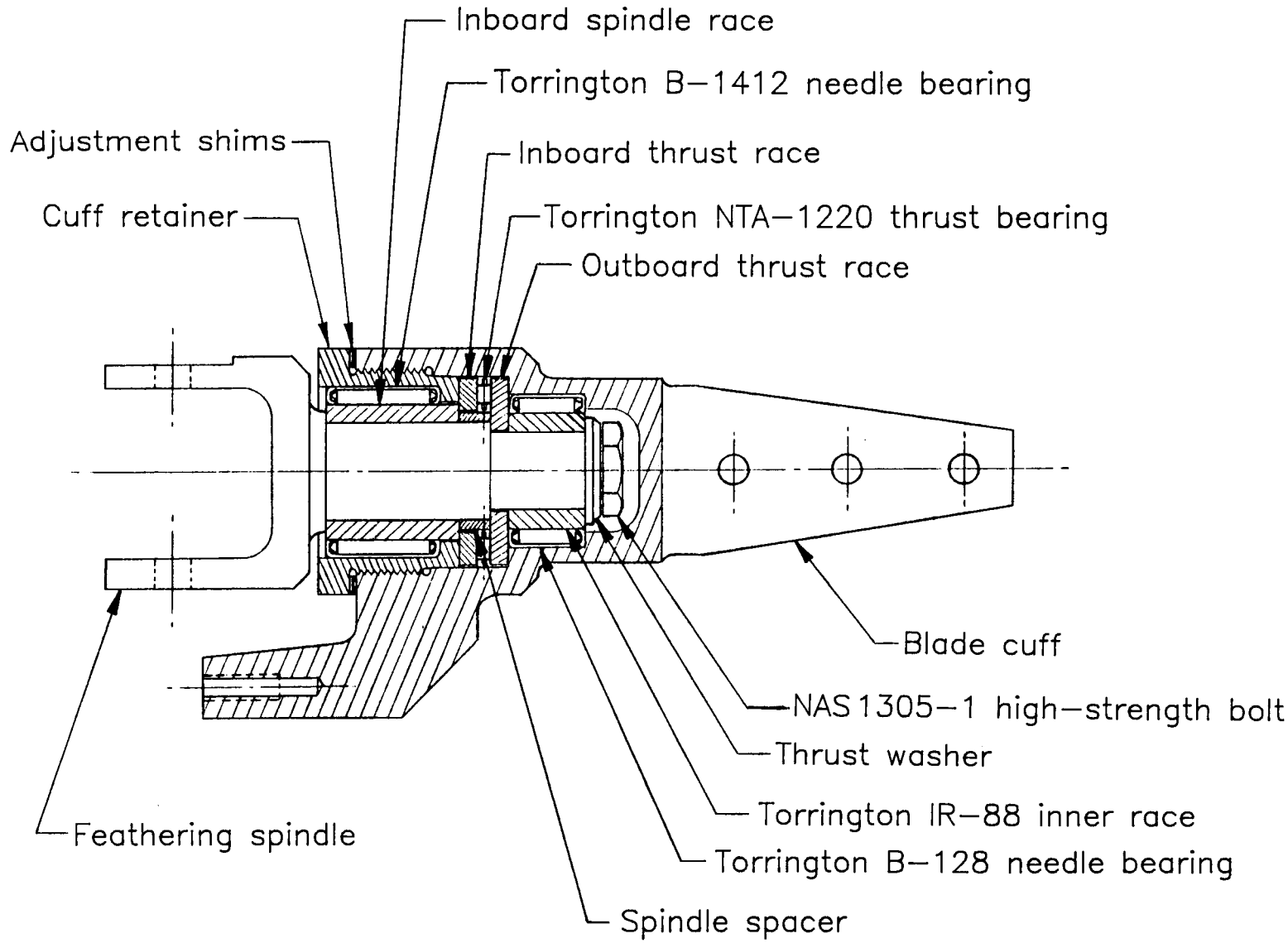

Figure 8. Details of blade cuff assembly.

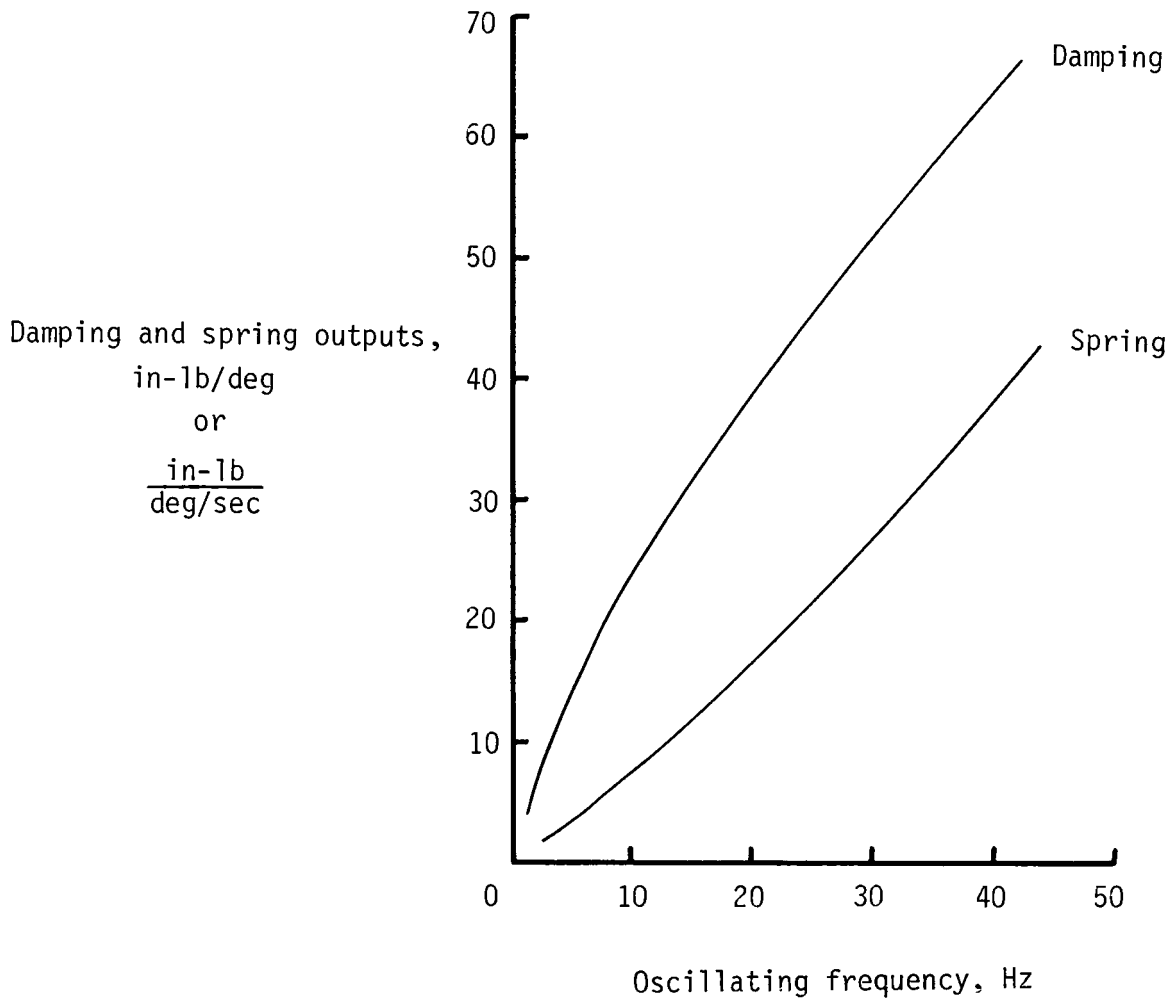

Figure 9. Inphase and quadrature characteristics of hub dampers for ±1° oscillation.

L-84-5501

(a) General arrangement of tapered-tip blade.

Figure 10. Typical rotor blade used on the 2MRTS. Dimensions are given in inches.

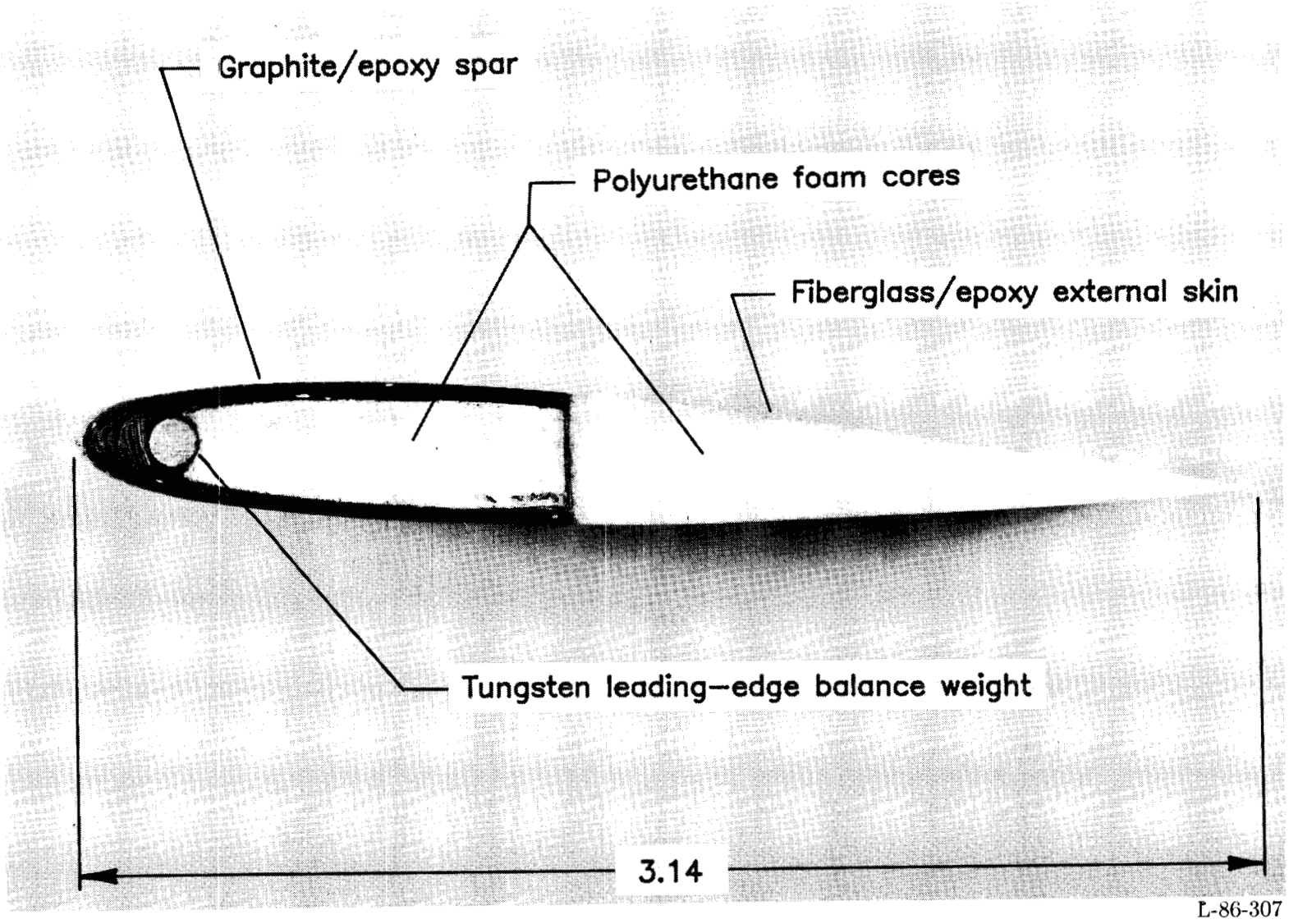

(b) Blade construction details.

Figure 10. Concluded.

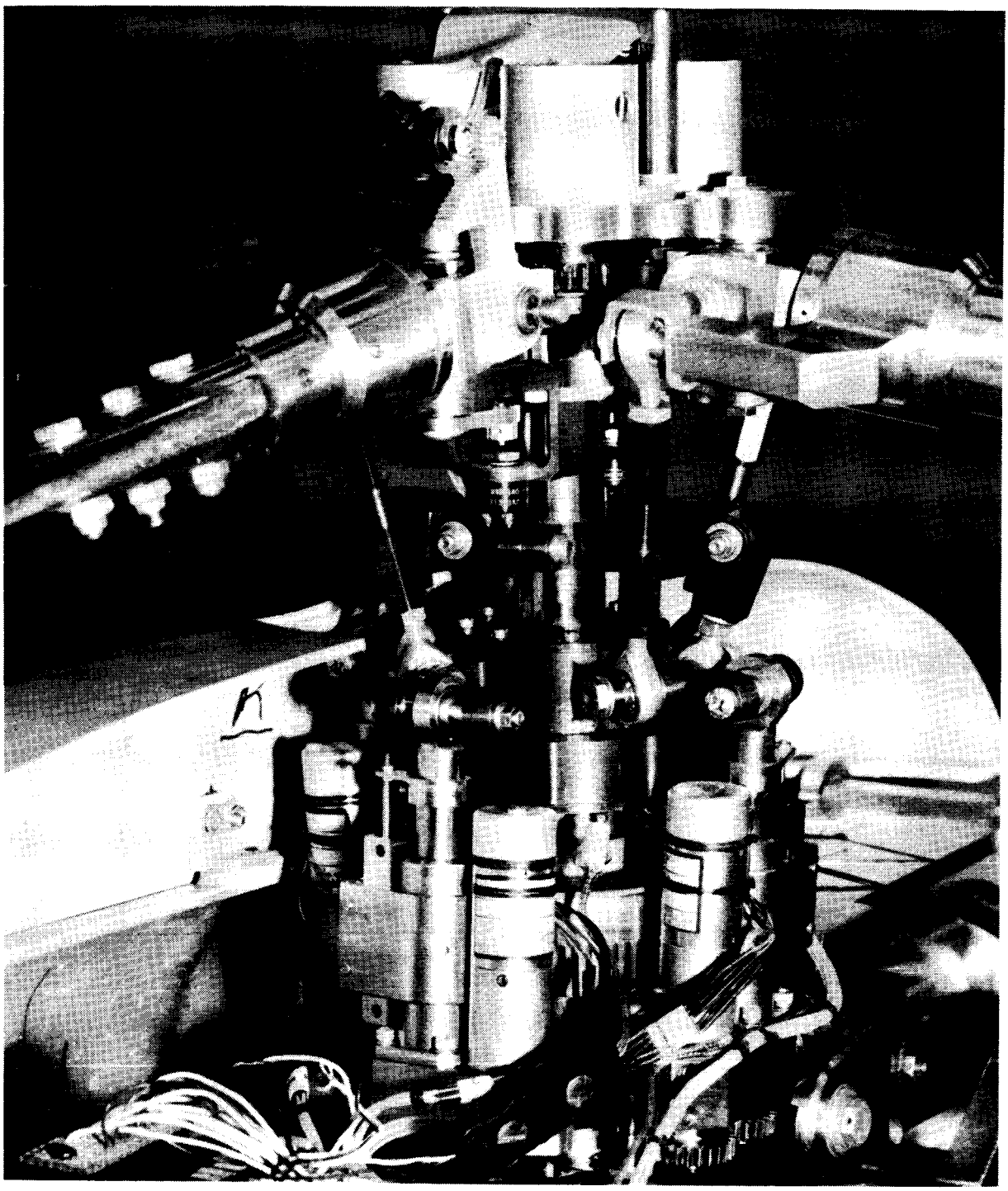

L-83-721

(a) Three-quarter front view.

Figure 11. Rotor control system.

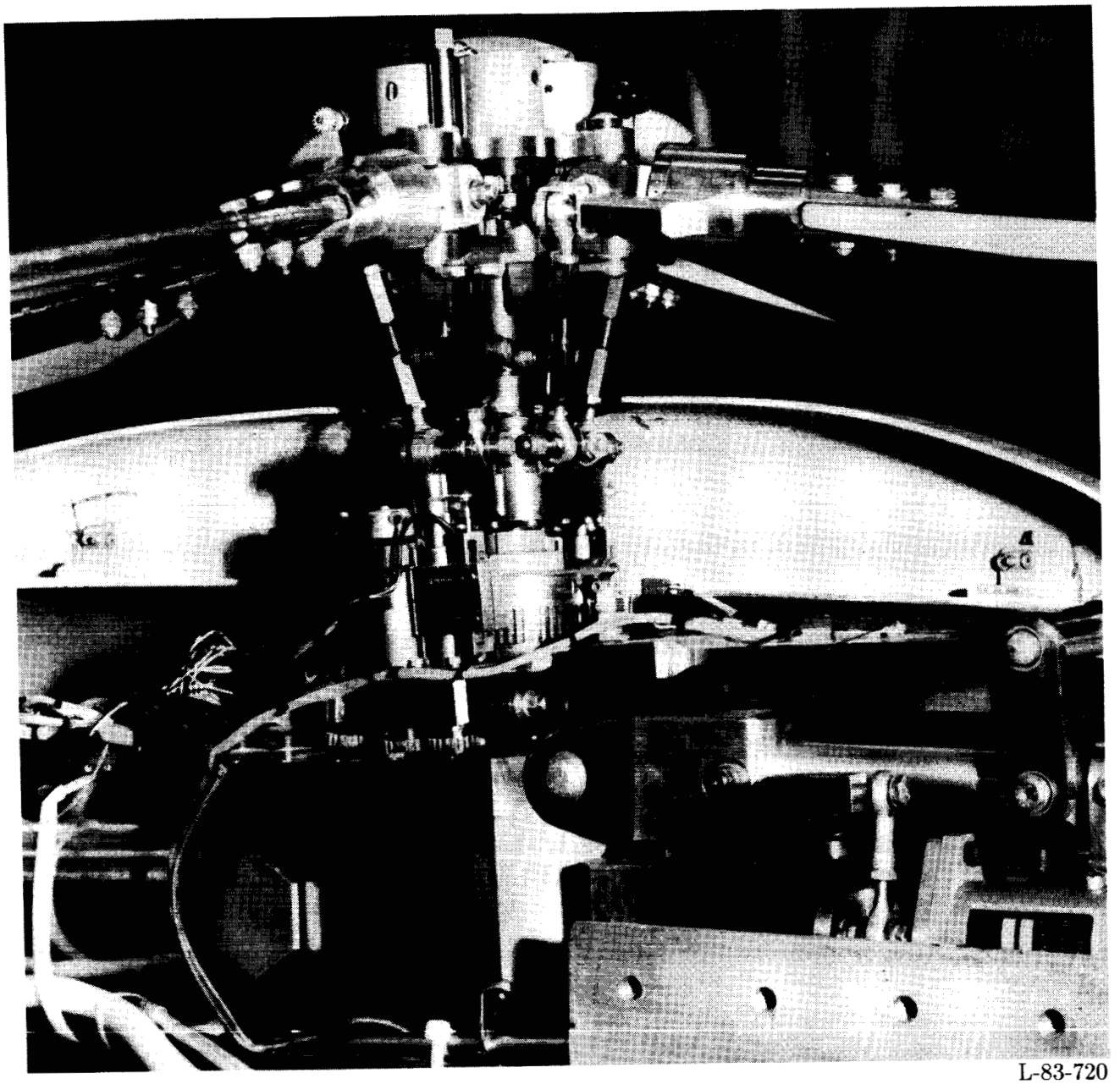

L-83-720

(b) Three-quarter rear view.

Figure 11. Concluded.

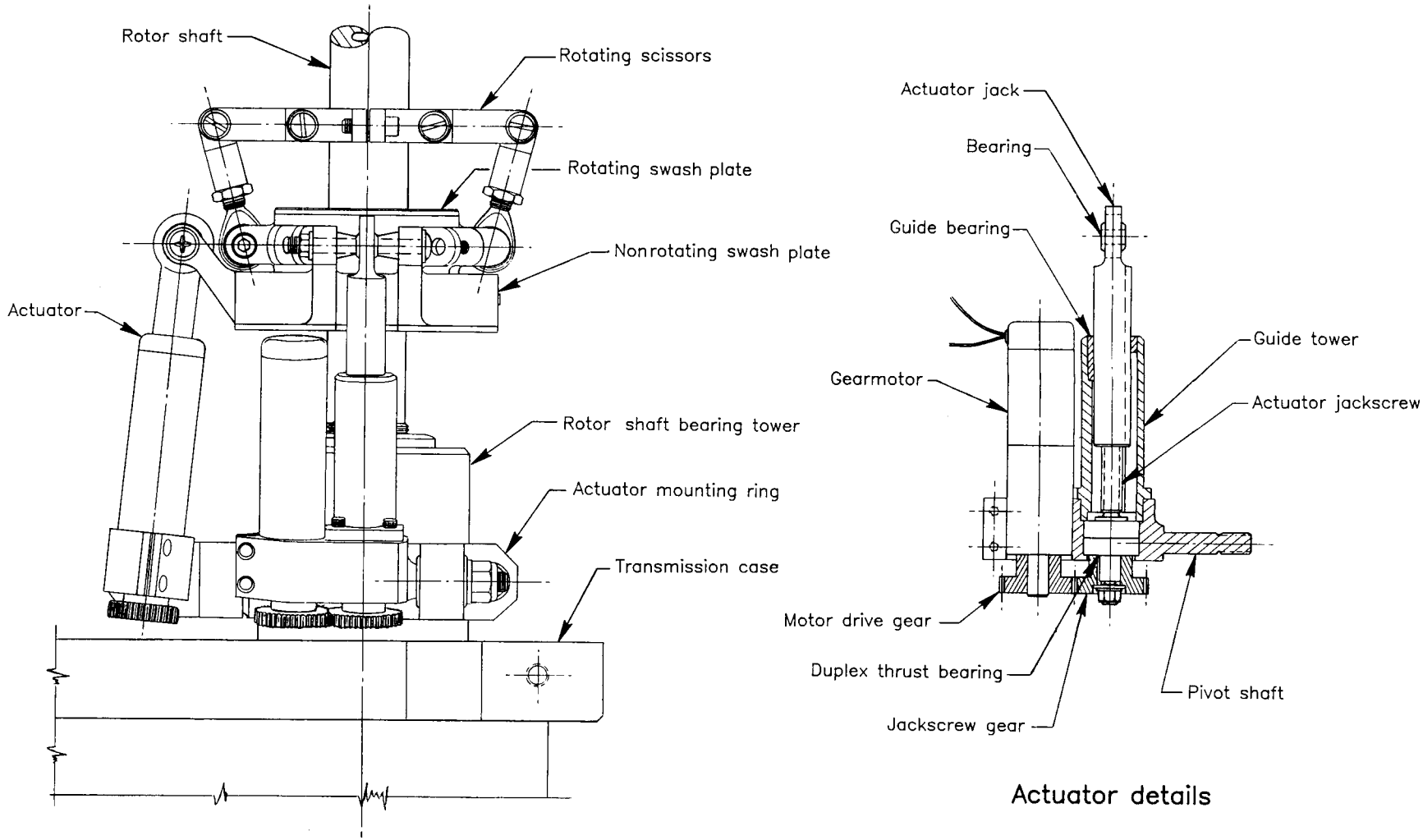

Figure 12. General arrangement of control system components.

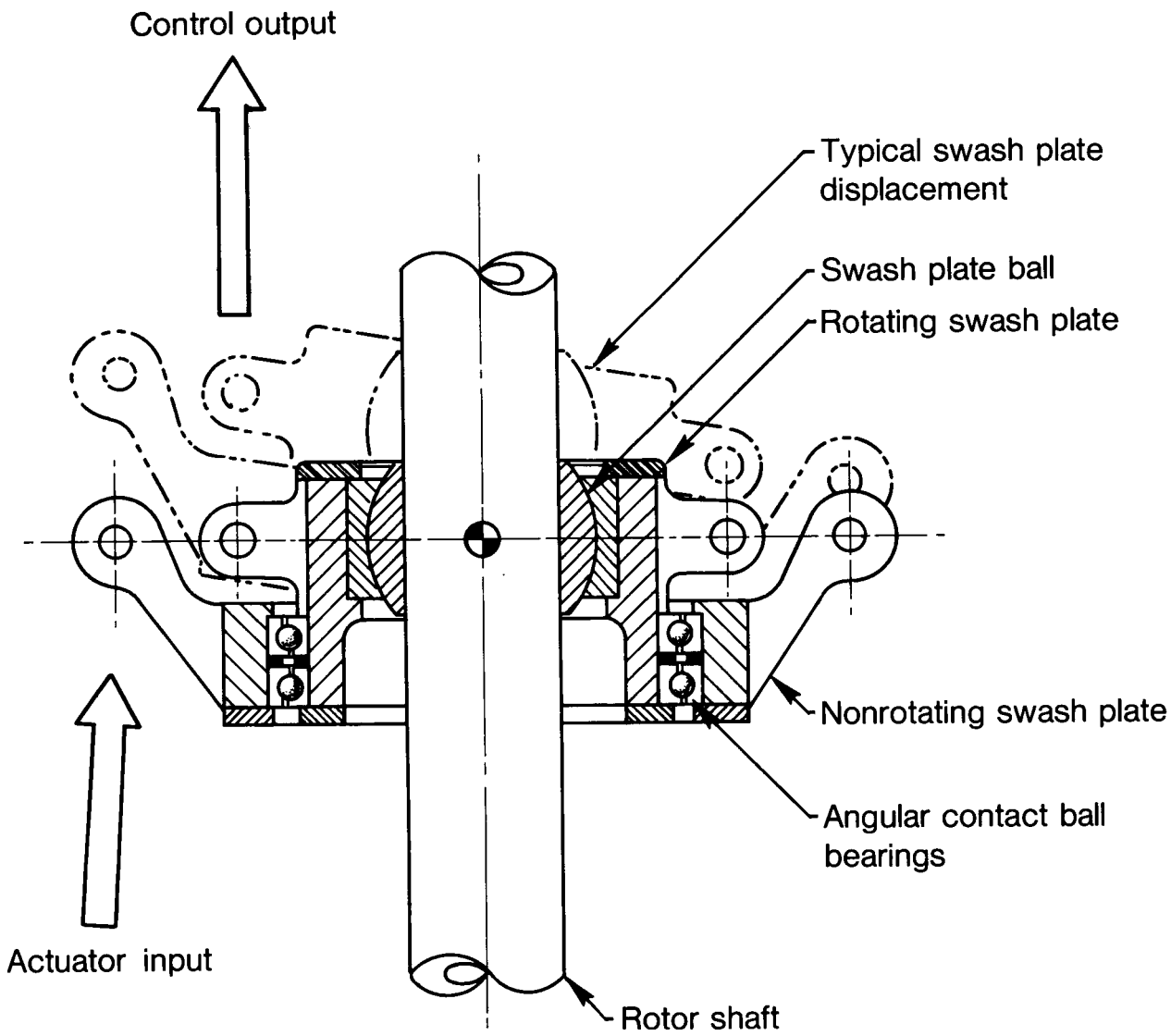

Figure 13. Swash plate details.

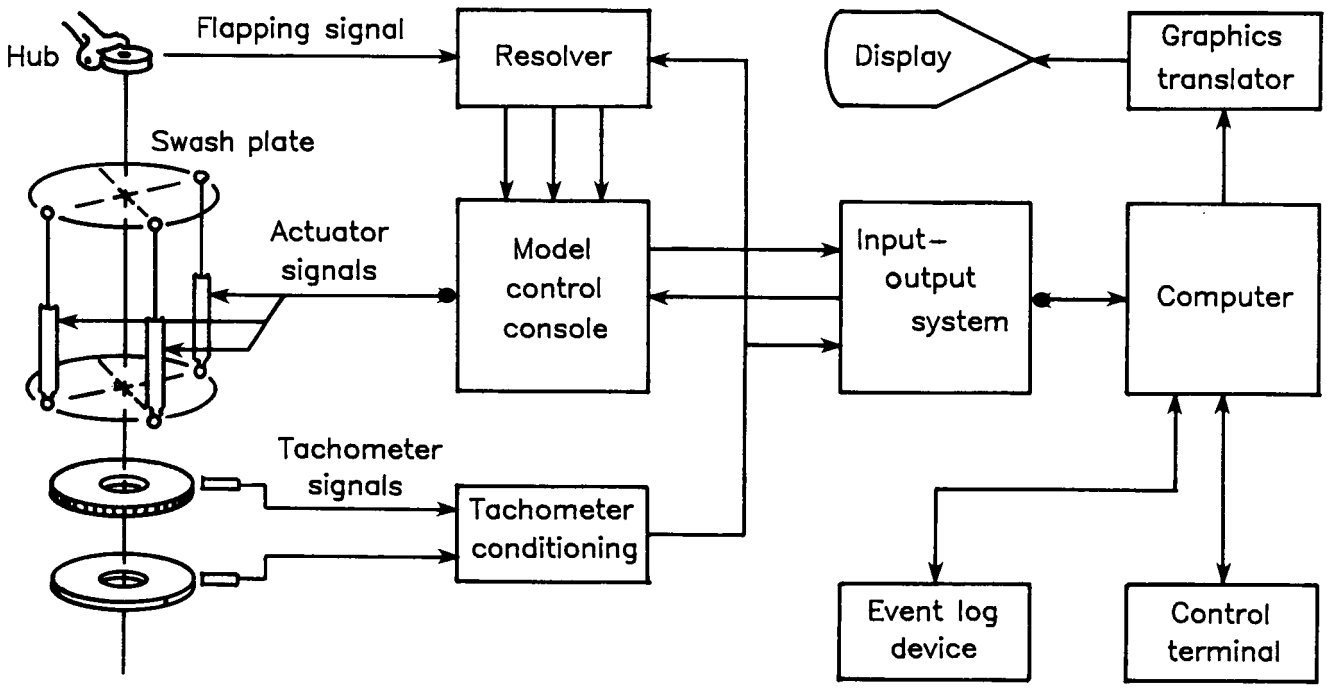

(a) Block diagram.

Figure 14. Model control system.

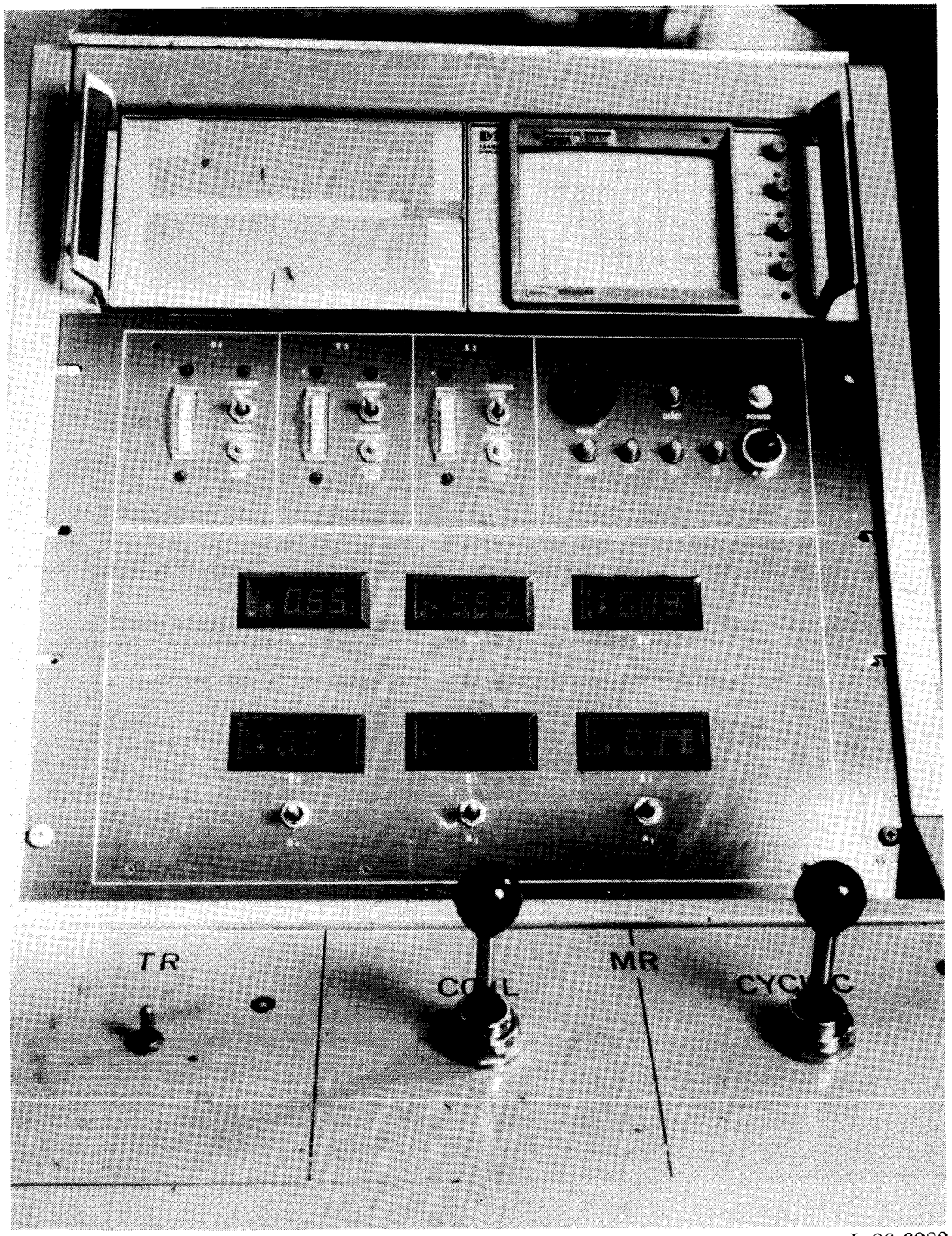

L-86-6982

(b) Control console.

Figure 14. Concluded.

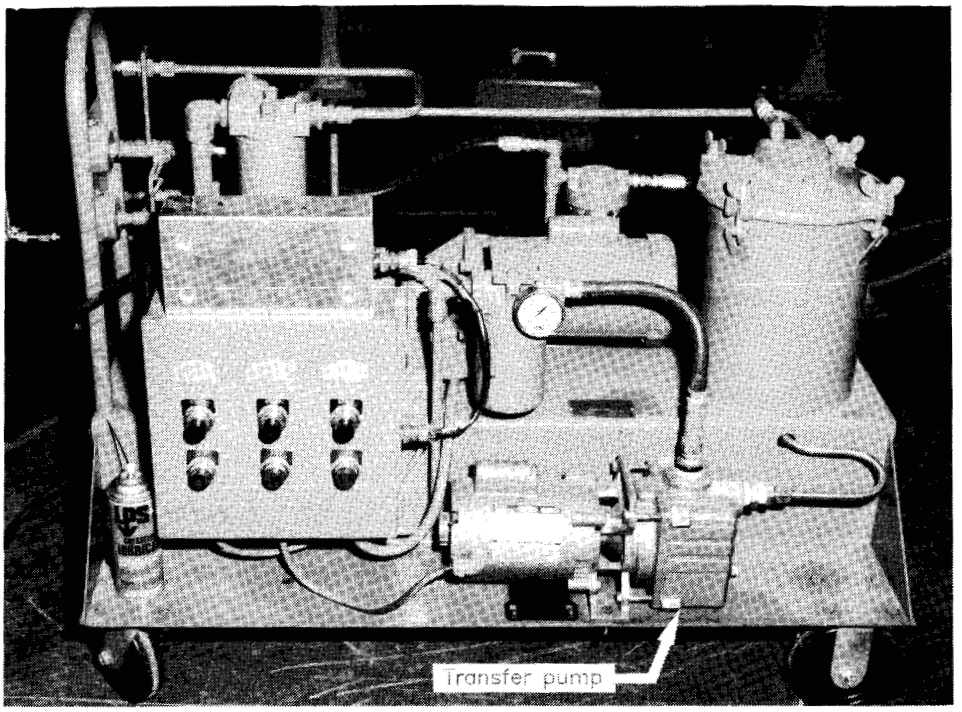

L-83-727

(a) Front view.

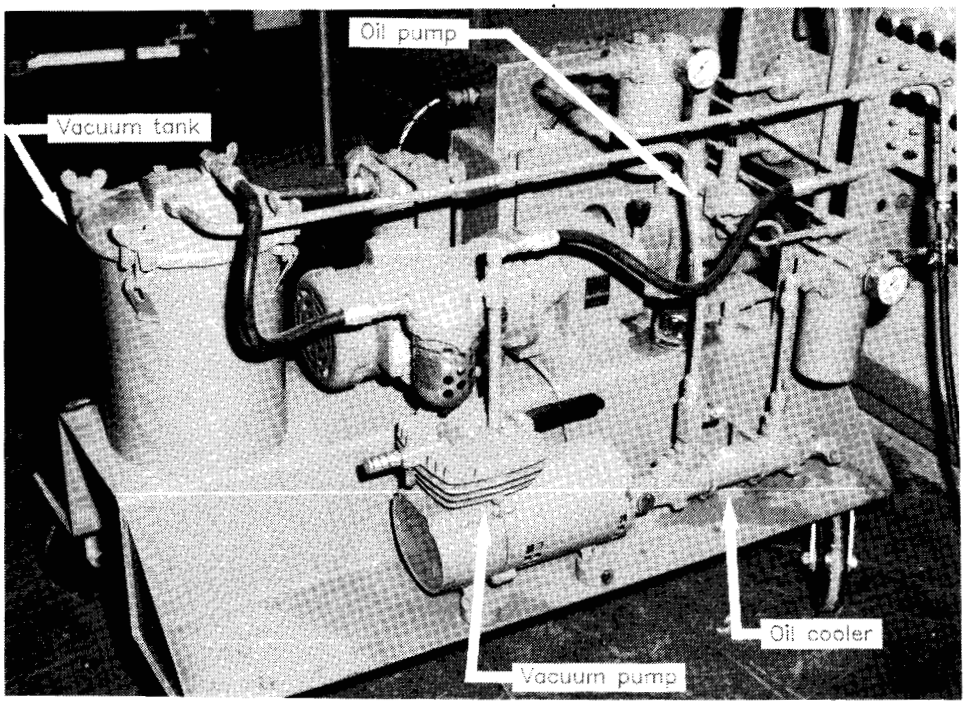

L-83-726

(b) Three-quarter rear view.

Figure 15. Lubrication system of transmission.

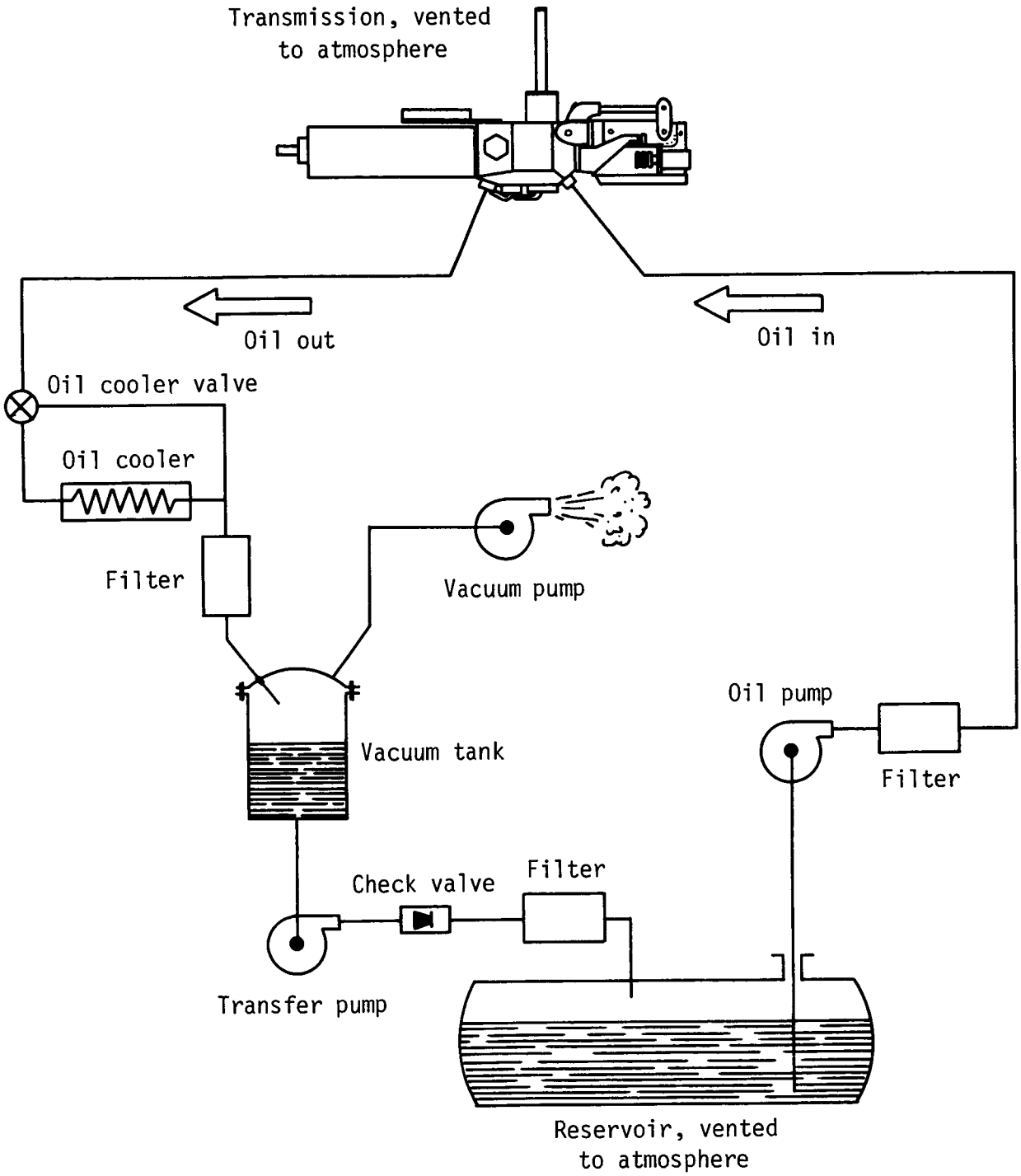

Figure 16. Schematic diagram of oil circuit through lubrication system of transmission.

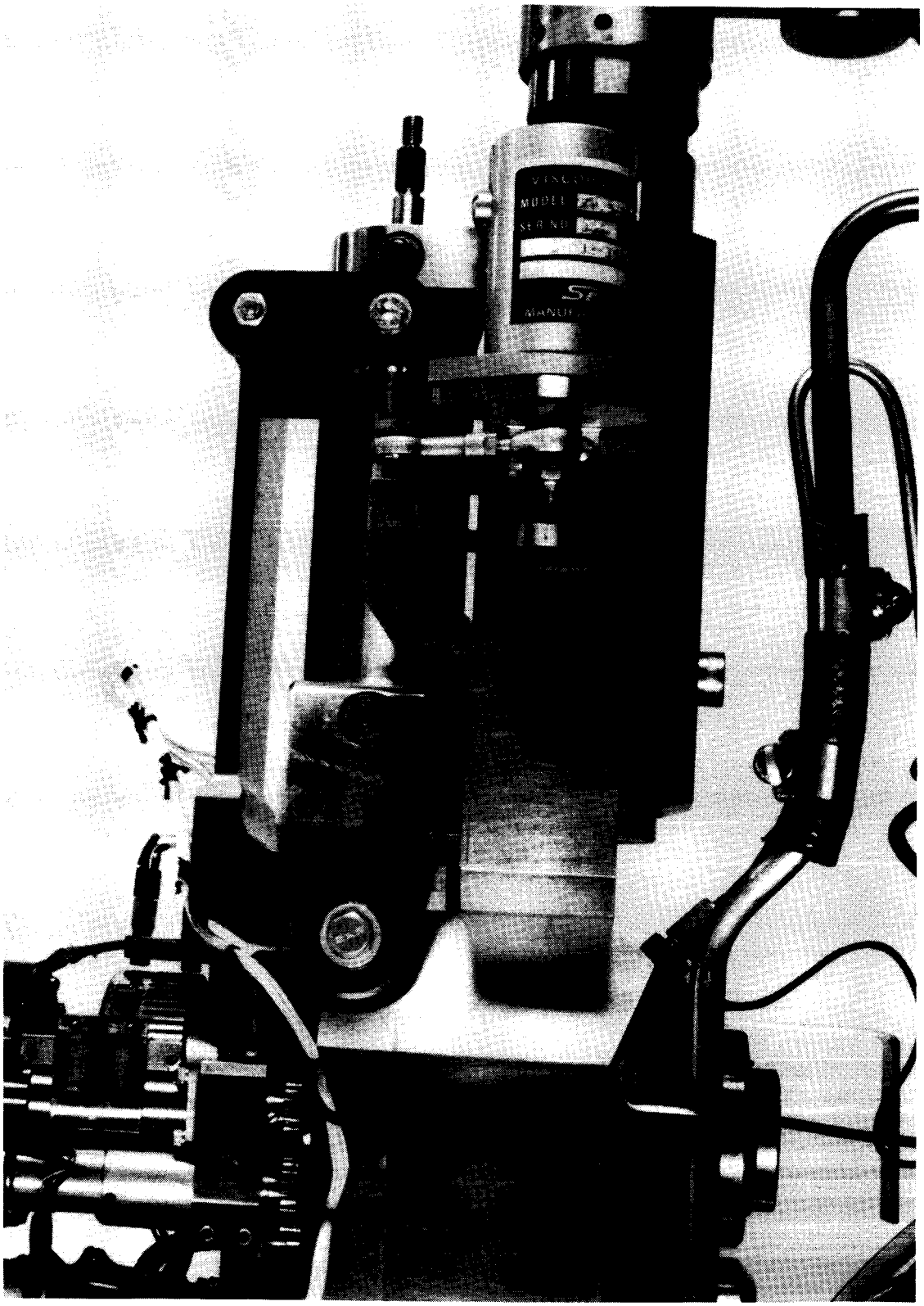

L-84-5548

Figure 17. Gimbal.

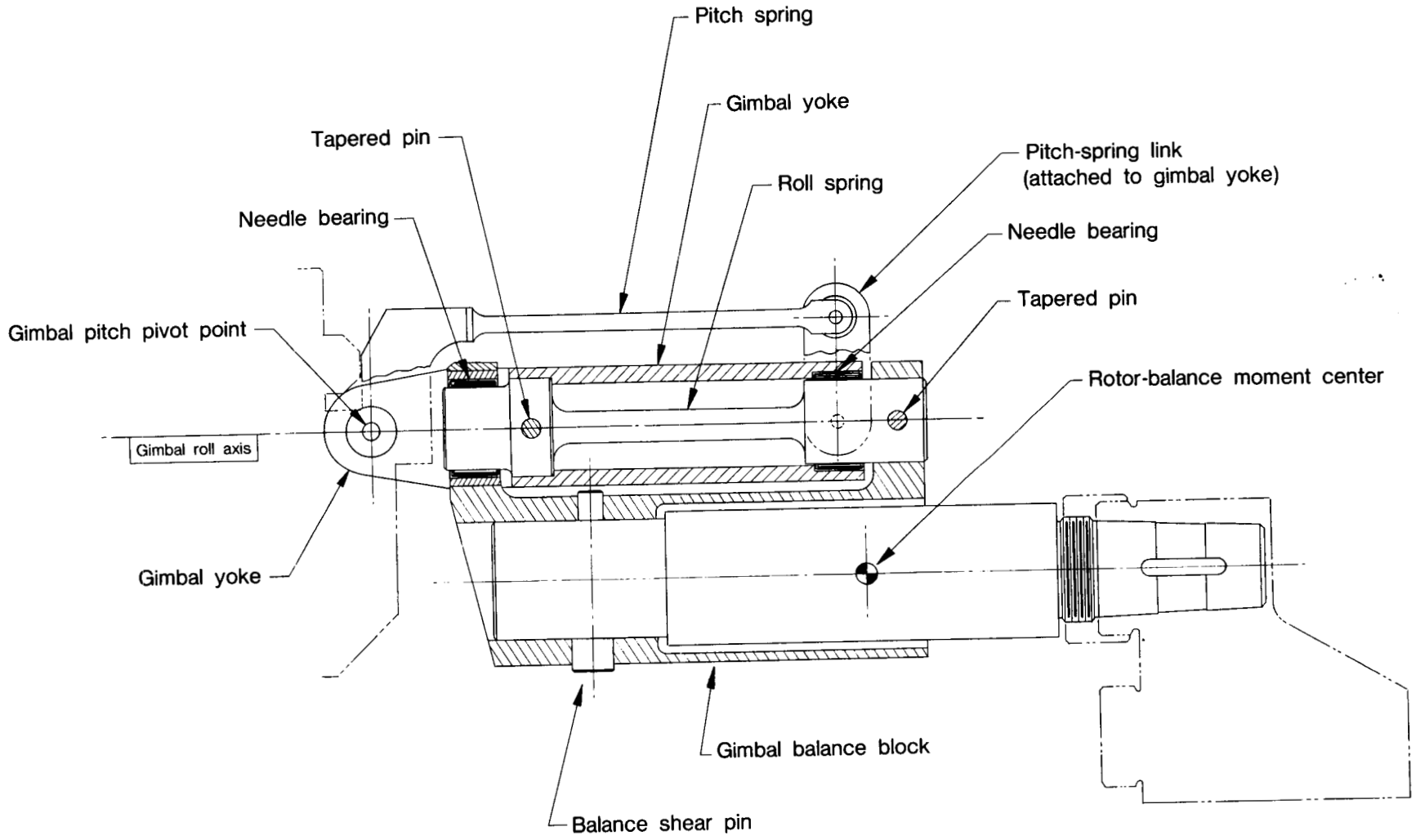

Figure 18. General arrangement of gimbal components.

L-83-723

Figure 19. General research fuselage used with the 2MRTS.

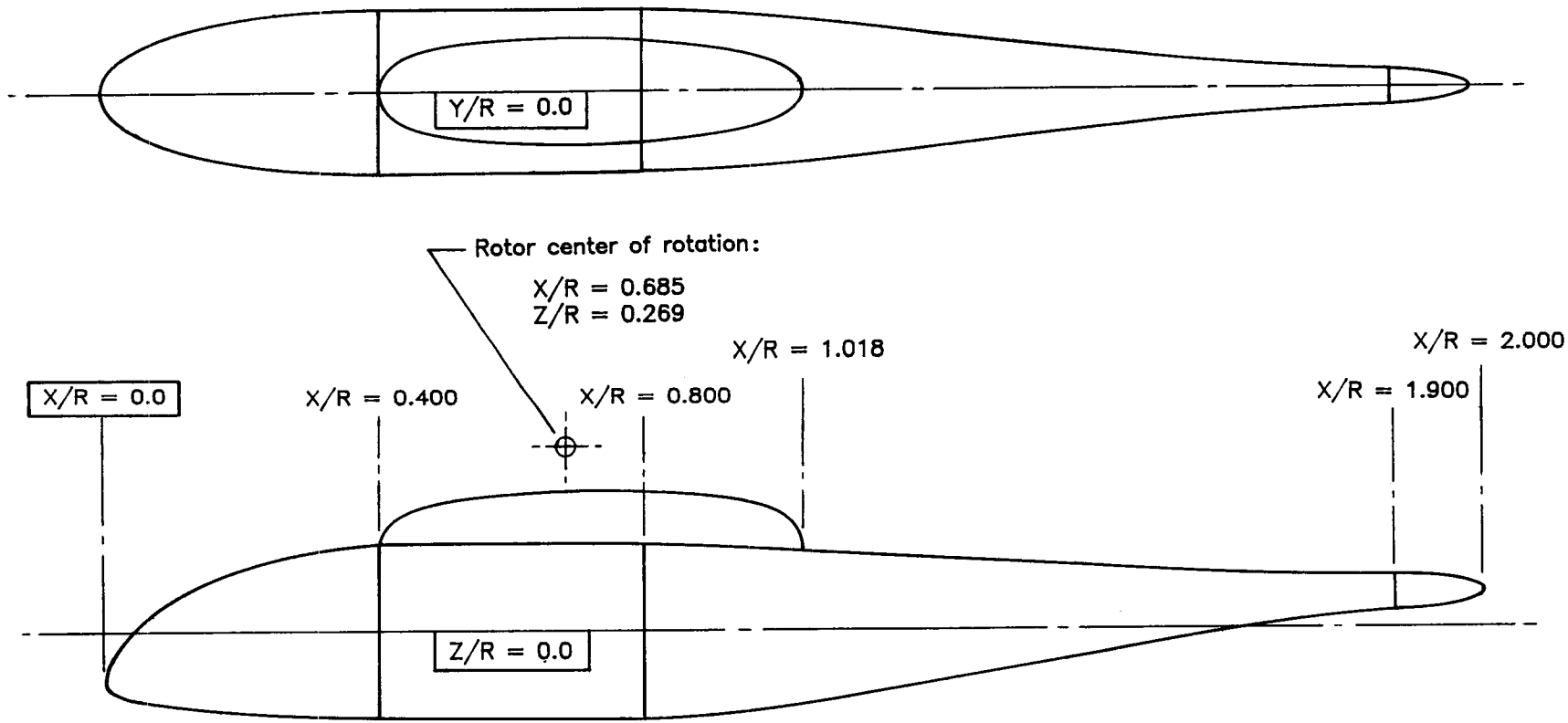

Figure 20. Fuselage component regions. (See appendix C.) Figure taken from reference 4.

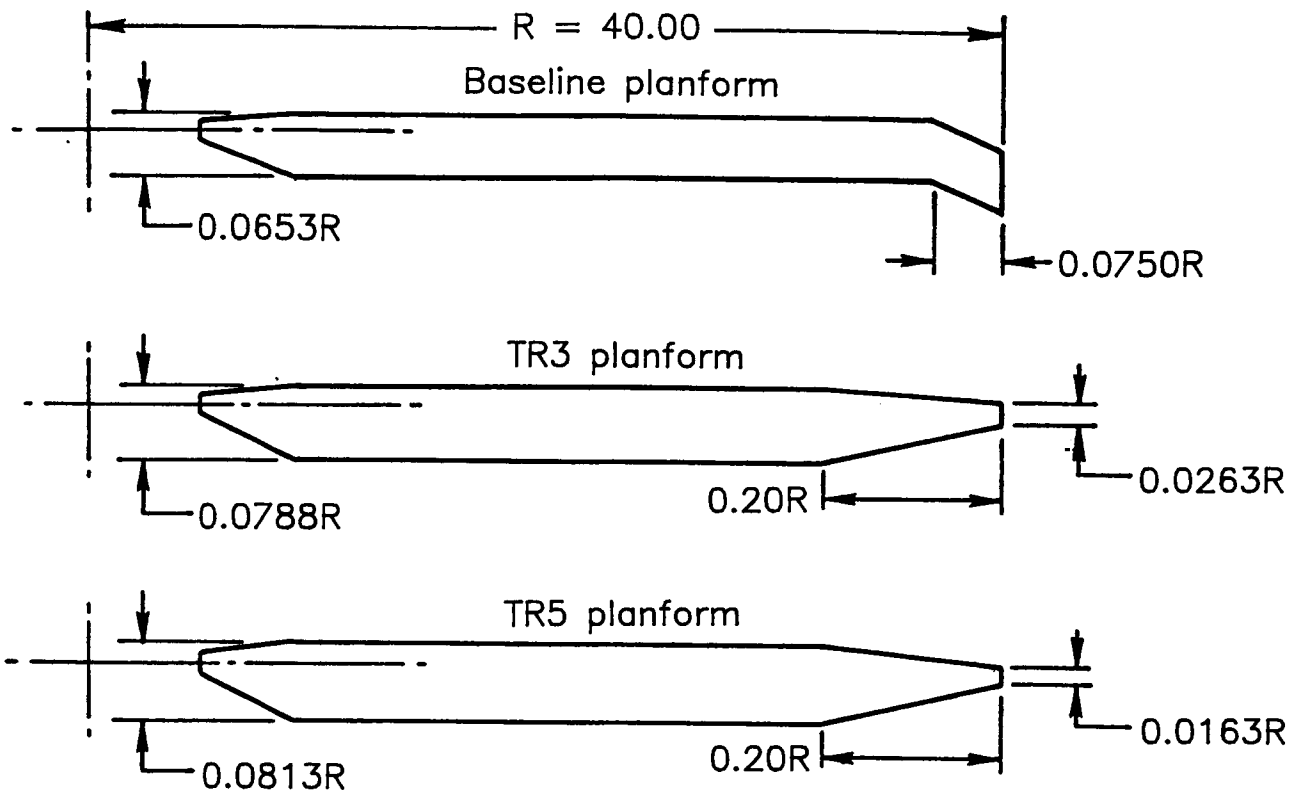

Planform	Twist, deg	Taper ratio	Tip sweep, deg
Baseline	−16 (nonlinear)	1:1	20 (aft)
TR3	−16	3:1	0
TR5	−16	5:1	0

Figure 21. Blade planform details. NACA 0012 airfoil section used for all blades; figure taken from reference 5; $\sigma_T = 0.0825$. Linear dimensions are given in inches.

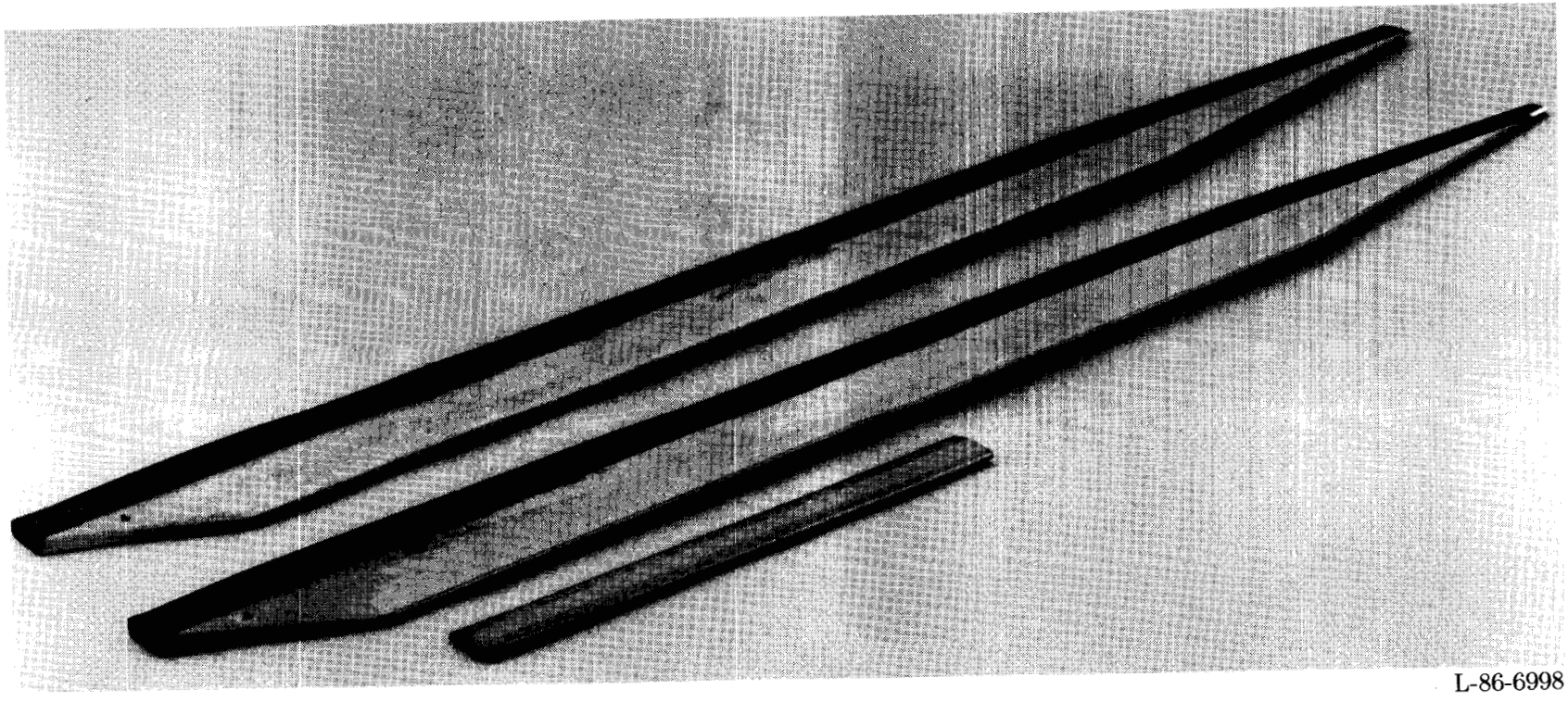

L-86-6998

Figure 22. Rotor blades of tapered composite-construction model. Span of blades is approximately 35 in.; chord of rectangular portion of blades is slightly over 3 in.

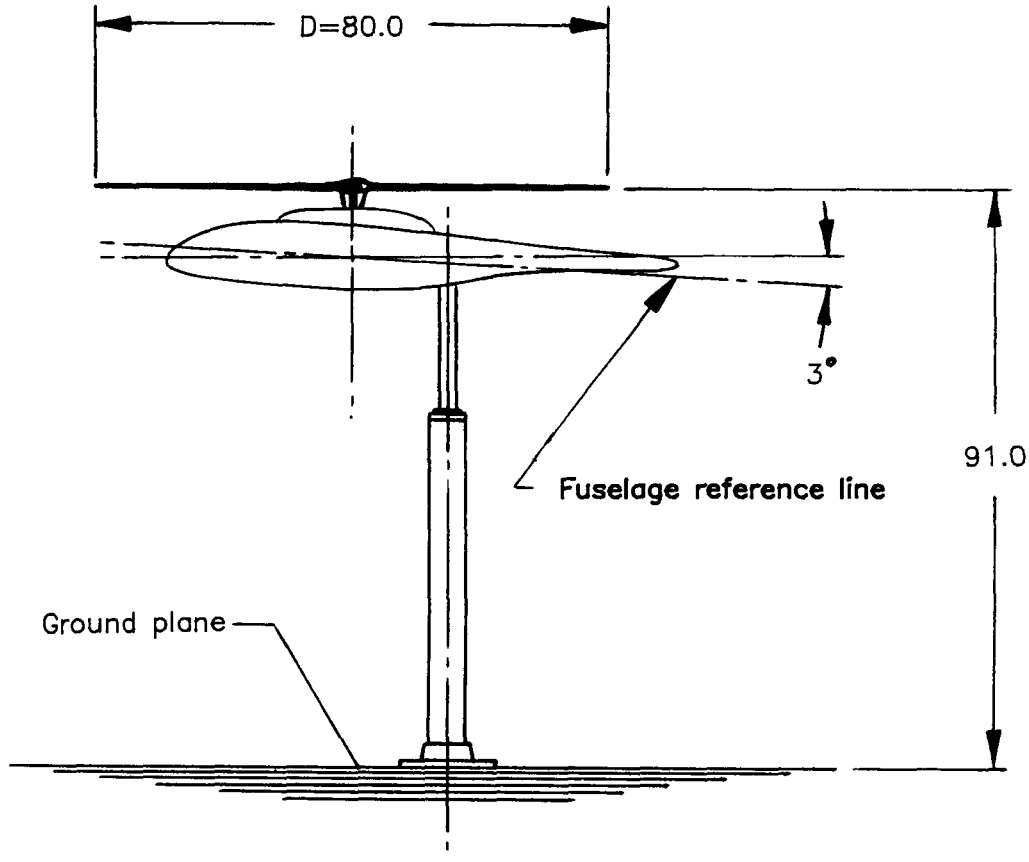

Figure 23. Mounting arrangement of the 2MRTS. Dimensions are given in inches unless otherwise specified.

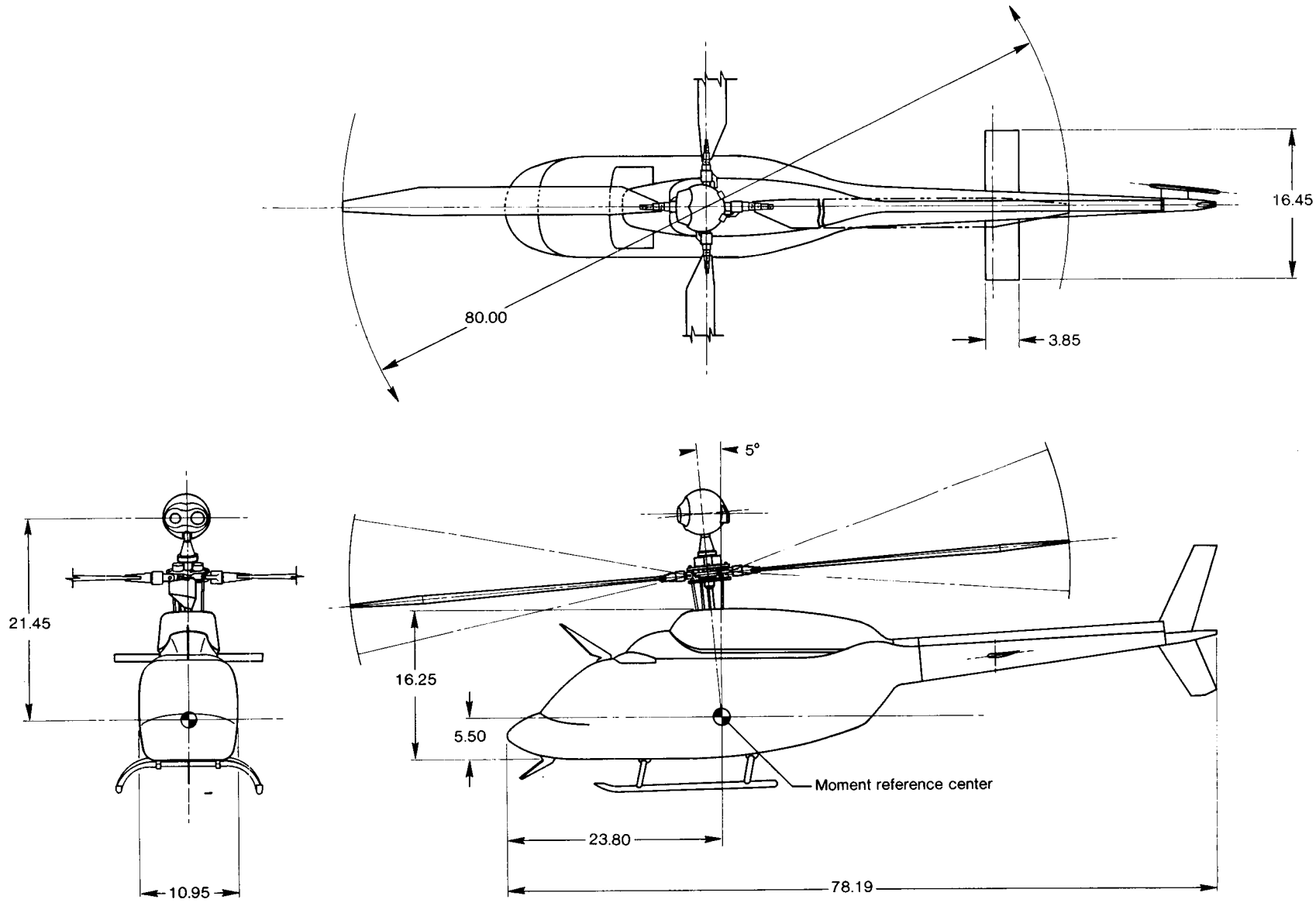

(a) General arrangement. Dimensions are given in inches unless otherwise specified.

Figure 24. Model of U.S. Army scout helicopter used in wind-on tests.

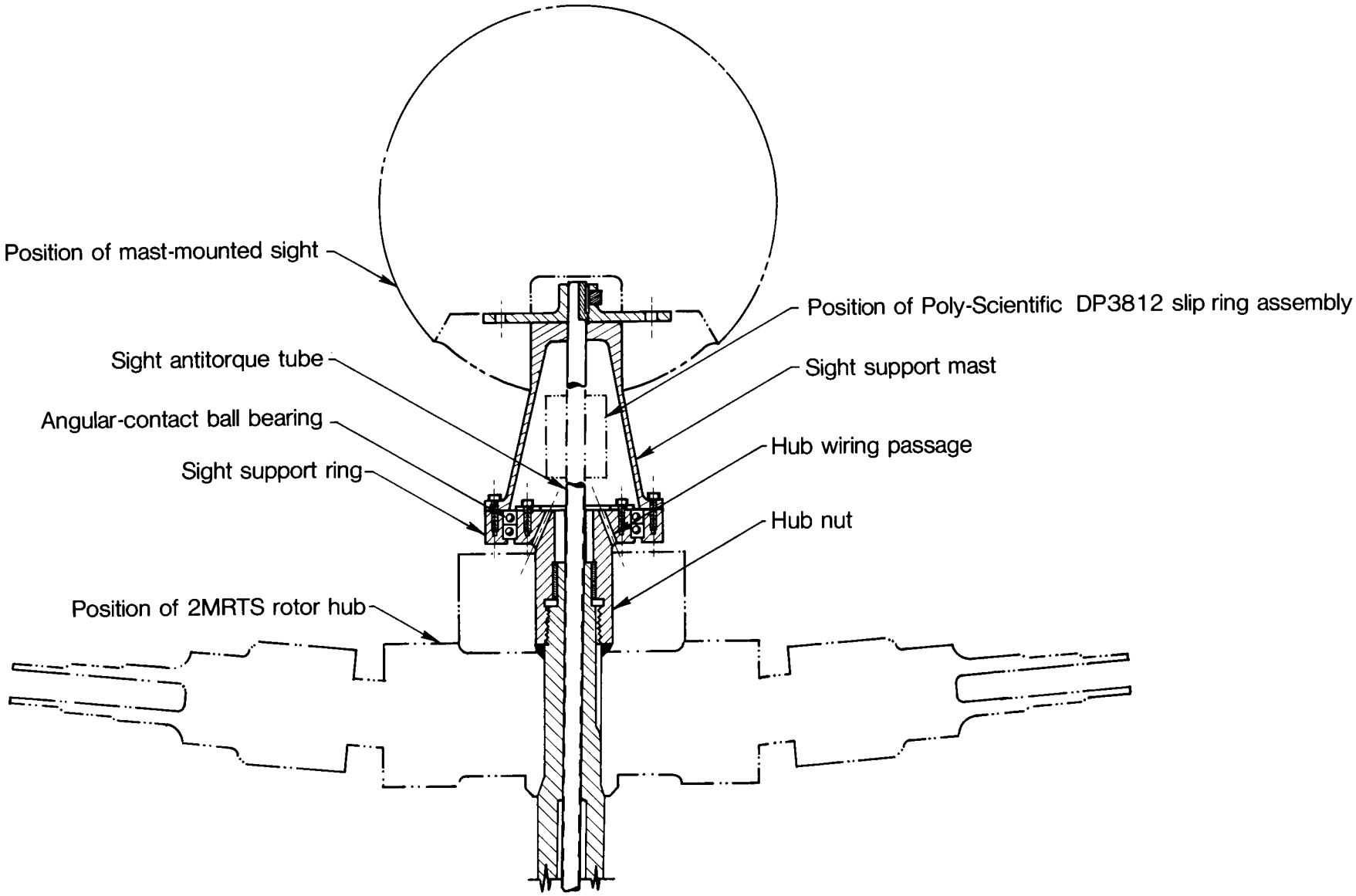

(b) Hub nut and support for mast-mounted sight.

Figure 24. Continued.

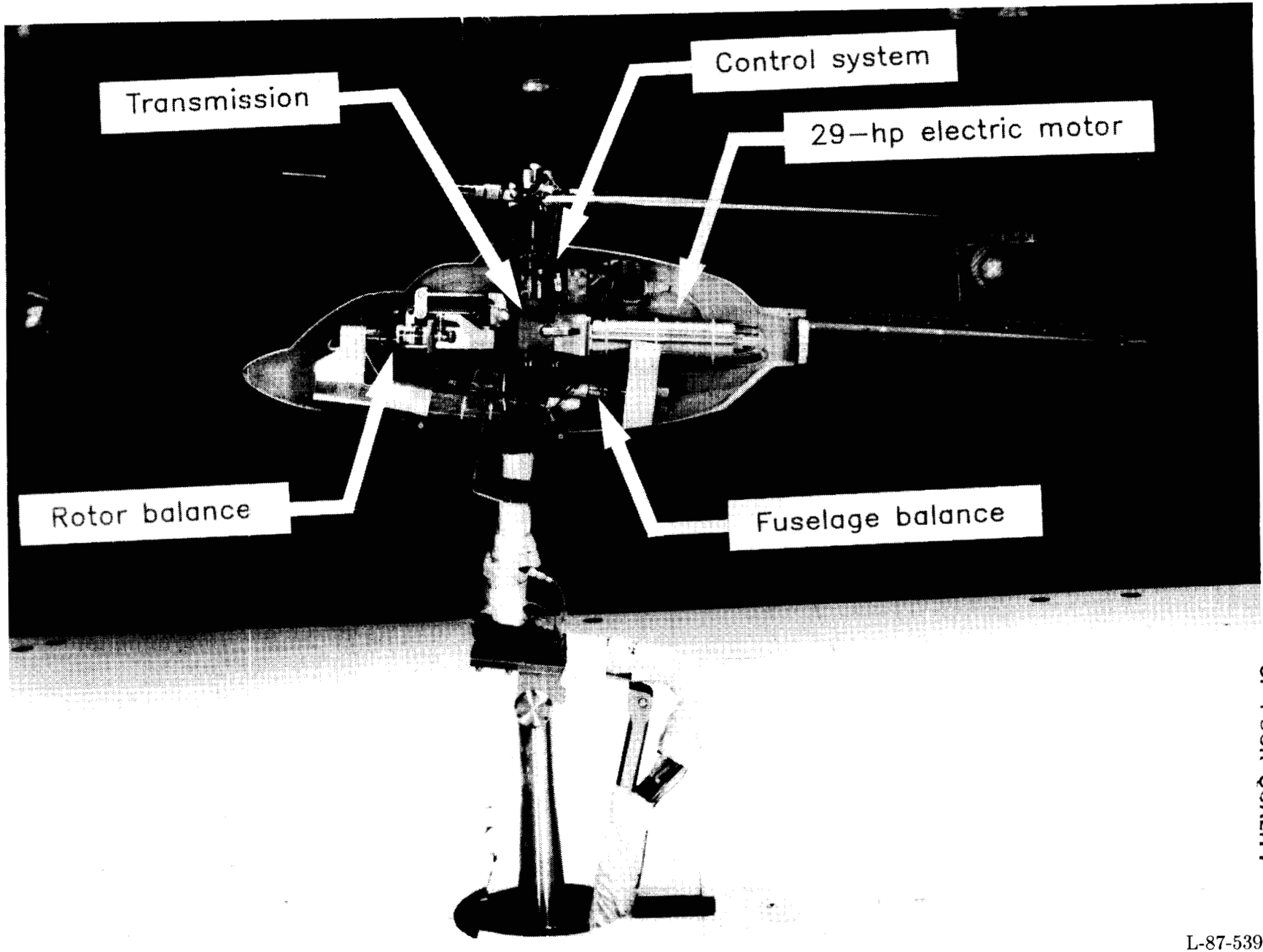

L-87-539

(c) Internal arrangement of the 2MRTS mounted in U.S. Army scout helicopter model.

Figure 24. Continued.

L-84-308

(d) U.S. Army scout helicopter mounted in the Langley 4- by 7-Meter Tunnel.
Figure 24. Concluded.

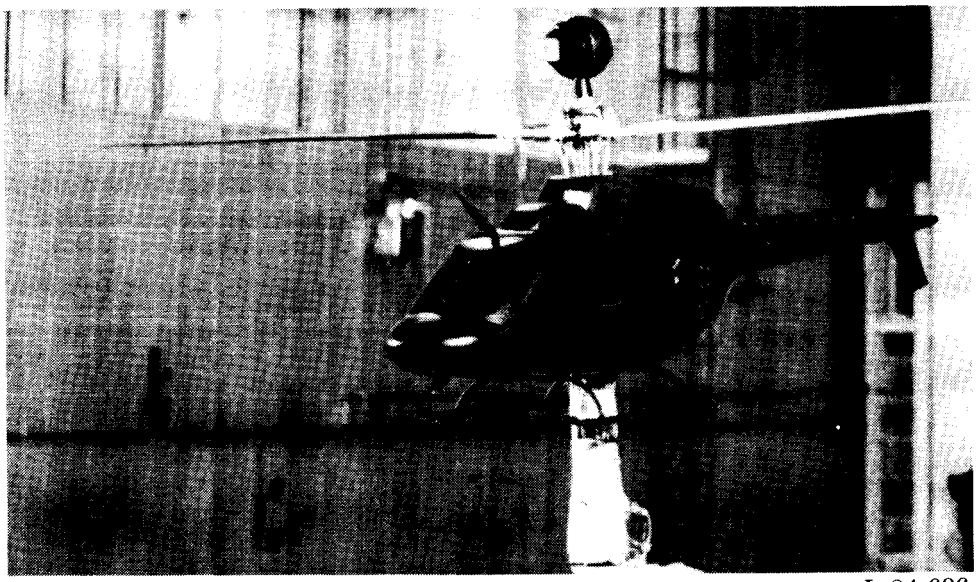

L-84-606

(a) MMS on.

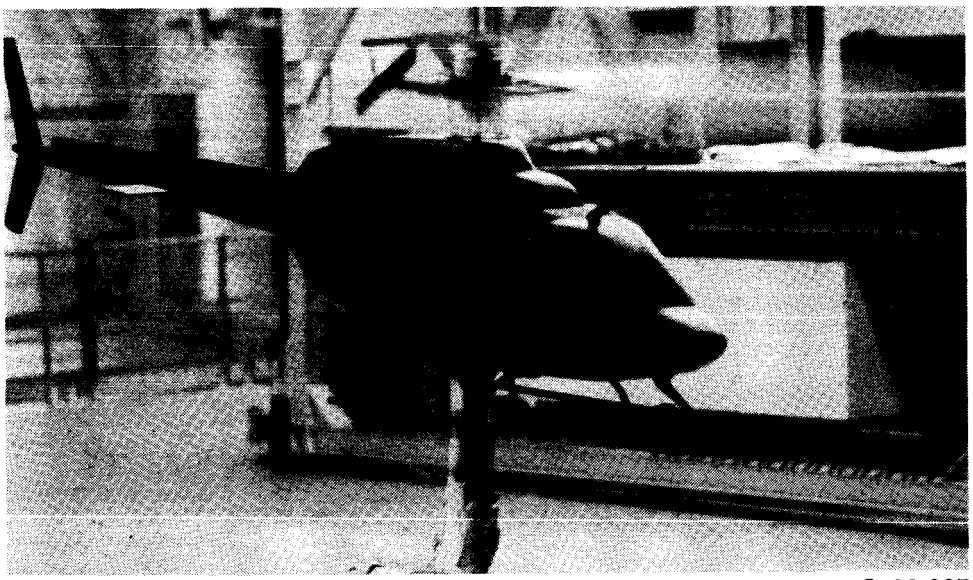

L-86-387

(b) MMS off.

Figure 25. Model operating in the Langley 4- by 7-Meter Tunnel.

(a) $\mu = 0.04$.

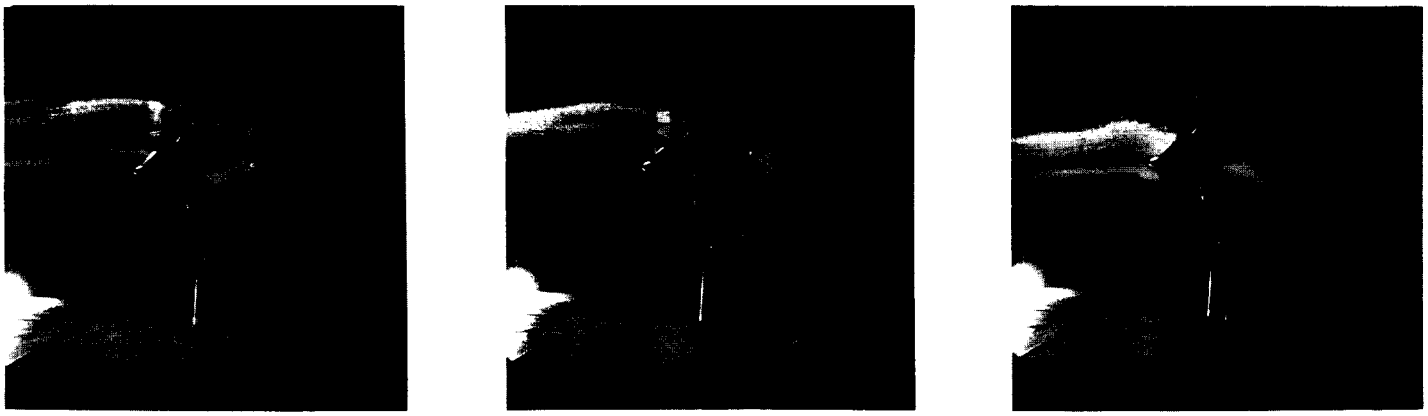

(b) $\mu = 0.08$.

L-86-388

Figure 26. Smoke-flow photographs taken during tests of scout helicopter. $C_T/\sigma = 0.0776$.

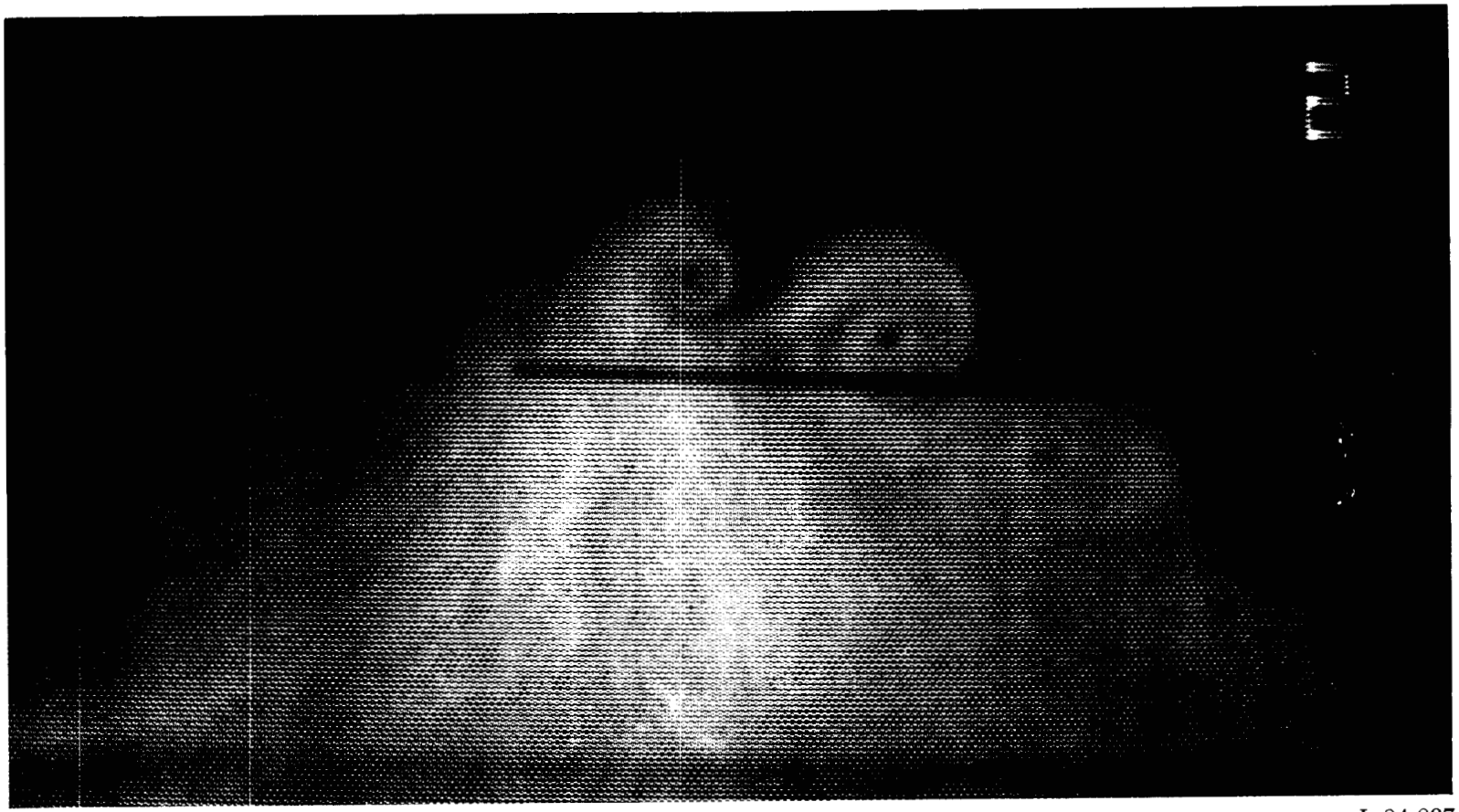

L-84-807

Figure 27. Photograph of video monitor screen showing path of blade-tip vortex over leading edge of rotor disk. $\mu = 0.04$; $C_T = 0.0064$.

Standard Bibliographic Page

1. Report No.	2. Government Accession No.	3. Recipient's Catalog No.
NASA TM-87762 AVSCOM TM 86-B-4		

4. Title and Subtitle	5. Report Date
Description of the U.S. Army Small-Scale 2-Meter Rotor Test System	February 1987
	6. Performing Organization Code: 505-61-51-10
7. Author(s): Arthur E. Phelps III and John D. Berry	8. Performing Organization Report No.: L-16165
9. Performing Organization Name and Address: Aerostructures Directorate, USAARTA-AVSCOM, Langley Research Center, Hampton, VA 23665-5225	10. Work Unit No.
	11. Contract or Grant No.
12. Sponsoring Agency Name and Address: National Aeronautics and Space Administration, Washington, DC 20546-0001 and U.S. Army Aviation Systems Command, St. Louis, MO 63120-1798	13. Type of Report and Period Covered: Technical Memorandum
	14. Army Project No.: 1L161102AH45

15. Supplementary Notes

Arthur E. Phelps III and John D. Berry: Aerostructures Directorate, USAARTA-AVSCOM.

16. Abstract

A small-scale powered rotor model was designed for use as a research tool in the exploratory testing of rotors and helicopter models. The model, which consists of a 29-hp rotor drive system, a four-blade fully articulated rotor, and a fuselage, was designed to be simple to operate and maintain in wind tunnels of moderate size and complexity. Two six-component strain-gauge balances are used to provide independent measurement of the rotor and fuselage aerodynamic loads. Commercially available standardized hardware and equipment were used to the maximum extent possible, and specialized parts were designed so that they could be fabricated by normal methods without using highly specialized tooling. The model was used in a hover test of three rotors having different planforms and in a forward flight investigation of a 21-percent-scale model of a U.S. Army scout helicopter equipped with a mast-mounted sight.

17. Key Words (Suggested by Authors(s))	18. Distribution Statement
Rotor model Hover testing Rotor scaling	Unclassified—Unlimited Subject Category 02

19. Security Classif.(of this report)	20. Security Classif.(of this page)	21. No. of Pages	22. Price
Unclassified	Unclassified	63	A04

For sale by the National Technical Information Service, Springfield, Virginia 22161

NASA-Langley, 1987